Preoperative Planning for Conservative Robotic Hip Surgery

Mariana Correia dos Santos

Thesis to obtain the Master of Science Degree in

Biomedical Engineering

Supervisors: Prof. Jorge Manuel Mateus Martins

Prof. Dr. Paulo Amaral Rego

Examination Committee

Chairperson: Profª. Rita Homem de Gouveia Costanzo Nunes

Supervisor: Prof. Jorge Manuel Mateus Martins

Members of the Committee: Prof. João Carlos Prata dos Reis

October 2019

Preface

The work presented in this thesis was performed at the Surgical Robotics Lab (SRL) of IDMEC, Instituto Superior Técnico (Lisbon, Portugal), during the period February-October 2019, under the supervision of Prof. Jorge Martins from IST and the co-supervision of Dr. Paulo Rego from Hospital da Luz.

Declaração

Declaro que o presente documento é um trabalho original da minha autoria e que cumpre todos os requisitos do Código de Conduta e Boas Práticas da Universidade de Lisboa.

Declaration

I declare that this document is an original work of my own authorship and that it fulfils all the requirements of the Code of Conduct and Good Practices of the Universidade de Lisboa.

Abstract

Femoroacetabular impingement (FAI) is a medical condition that usually affects young athletes who suffer from hip pain during certain physical activities. Typically, the diagnosis is confirmed by radial magnetic resonance imaging (MRI) and it is treated during minimally invasive surgery: conservative hip surgery. This procedure requires an orthopedic surgeon with much experience, skill and dexterity, as the femoral head bone must be drilled to correct the loss of sphericity due to the cam type FAI. However, revision surgeries may be required mainly because of inappropriate bone resection, due to poor visualization or planning.

The current project features a preoperative planning tool to be part of a robot-assisted conservative hip surgery. With robotic technology it is possible to perform more accurate movements, making results reproducible regardless of the surgeon, reducing variation in outcomes and improving patient safety. An interactive application was developed in MATLAB® in which the user can outline the contour of a healthy femoral head over each 2D radial MRI view of the unhealthy femur in a user-friendly and easy-to-view manner. In addition, the software can successfully create the 3D surface correspondent to the limits of the region to operate which will act as safety zone in which the robot arm will be constrained to work. Lastly, with the help of the optical measurement technology NDI Polaris Spectra System the registration between this surface and the surface of the real femoral head was completely mapped and calculated using the Iterative Closest Point algorithm with an error of the order of 2mm.

Keywords: Femoroacetabular Impingement; radial MRI; Preoperative Surgical Planning; Registration

Resumo

O conflito femoro-acetabular (CFA) é uma condição médica que afeta geralmente jovens atletas que sentem dor na anca durante determinadas atividades físicas. Normalmente, o diagnóstico é confirmado por imagens de ressonância magnética radiais e é tratado durante a cirurgia minimamente invasiva: conservadora da anca. Este procedimento requer um cirurgião ortopédico com muita experiência, habilidade e destreza, pois a cabeça do fémur tem de ser desgastada de forma a corrigir a falta de esfericidade que é devido ao CFA do tipo cam. No entanto, em certos casos são necessárias cirurgias de revisão por inadequada resseção óssea, devido à falta de visualização ou planeamento na cirurgia.

Este trabalho apresenta uma ferramenta de planeamento pré-operatório para fazer parte de uma cirurgia robótica conservadora da anca. Com esta tecnologia é possível realizar movimentos mais precisos, tornando os resultados reproduzíveis, independentemente do cirurgião, reduzindo a variação nos resultados e melhorando a segurança do paciente. Foi desenvolvida uma aplicação interativa no MATLAB®, na qual o utilizador pode delinear o contorno de uma cabeça femoral saudável sobre cada imagem de ressonância magnética radial 2D do fémur não saudável, de forma intuitiva e de fácil visualização. Além disso, o software pode criar com sucesso a superfície 3D que corresponde aos limites da região a ser operada, que atuará como zona de segurança na qual o braço robótico será obrigado a trabalhar. Por fim, com a ajuda da tecnologia de medição óptica *NDI Polaris Spectra System*, o registo entre essa superfície e a superfície da cabeça femoral real foi completamente mapeado e calculado usando o algoritmo *iterative closest point* com um erro na ordem de 2 mm.

Palavras-chave: Conflito Femoro-Acetabular; Ressonância Magnética Radial; Planeamento Pré-operatório Cirúrgico; Registo

Acknowledgments

Sendo esta Tese o fruto de muitas horas de trabalho, é importante para mim exprimir os meus agradecimentos a todas as pessoas que de alguma forma contribuíram para o meu sucesso.

Ao meu orientador, Professor Jorge Martins, agradeço o acompanhamento e partilha de conhecimento sobre o tema tão vasto que é a Cirurgia Robótica.

Ao meu co-orientador, Prof. Dr. Paulo Rego, agradeço a oportunidade única de assistir à cirurgia conservadora da anca no Hospital da Luz que me permitiu contactar com a realidade e compreender melhor o papel do Engenheiro Biomédico no ramo da Cirurgia Ortopédica.

Ao pessoal do laboratório, obrigada pela companhia e ajuda ao longo destes meses.

Não podia deixar de mencionar todos os meus colegas do curso de Engenharia Biomédica que se tornaram grandes amigos e enriqueceram estes 5 anos que passei pelo Instituto Superior Técnico. Com especial destaque à Diana, Joana, Tuxinha, Helena e Pedro que tanto me apoiaram sempre com muito boa disposição.

À minha afilhada, Madalena, obrigada por acreditares em mim sempre com muito orgulho.

Agradeço também à minha malta de Massamá que me acompanha desde há muitos anos e que sempre confiou no meu potencial e me incentivou a ir mais longe, principalmente à Mafalda e Catarina pelas fugas à rotina do trabalho e estudo do Técnico.

A toda a minha família um especial obrigado por sempre acreditarem em mim desde pequenina e me ajudarem a crescer enquanto mulher. Em especial, aos meus pais que me educaram a tornar-me uma melhor pessoa e proporcionaram as melhores condições que poderia imaginar tanto a nível familiar como académico. Ao meu irmão, Tiago, obrigado pelo apoio, proteção e ajuda do melhor mano mais velho.

Por fim, obrigado Mor por seres a pessoa tão carinhosa e atenciosa que esteve e está presente em todos os momentos, sejam eles bons ou maus. Obrigada pelo apoio incondicional, por acreditares sempre em mim e por toda a força que me transmites.

Por último, gostava de recordar o meu ‘irmãozinho’ de quatro patas Sammy pela companhia e carinho dos últimos 14 anos.

Contents

List of Figures

List of Tables

List of Acronyms

2D	Two-Dimensional
3D	Three-Dimensional
CT	Computed Tomography
DICOM	Digital Imaging and Communications in Medicine
FAI	Femoroacetabular Impingement
FS	Fat Suppressed
GUI	Graphical User Interface
ICP	Iterative Closest Point
MRI	Magnetic Resonance Imaging
NMR	Nuclear Magnetic Resonance
OR	Operating Room
PCA	Principal Component Analysis
PD	Proton Density
RCS	Reference Coordinate System
RMSE	Root Mean Square Error
RF	Radio Frequency
TSE	Turbo Spin Echo

List of Symbols

$\mathbf{d_k}$	Mean square error
M	Transformation Matrix
$\mathbf{N_P}$	Number of points in data shape
$\mathbf{N_X}$	Number of points in model shape
P	Data shape
R	Rotation Matrix
t	Translation Vector
X	Model shape
$\boldsymbol{\tau}$	Tolerance

1. Introduction

1.1. Motivation

Technology is constantly evolving and in the medical field it is not an exception. Orthopedists are eager for better and more accurate procedures that can help them perform faster and safer surgeries, with better outcomes. Thus, medical robots have gained particular interest over the last 20 years as they can reproduce more precise movements, allowing them to work in the safety zone with more controlled cutting and milling without damaging the surrounding tissues. Also, robotic technology has been facilitating minimally invasive surgeries, which have recently gained popularity and as it reduces the variation in outcomes, as results are reproducible regardless of surgeon and patient. In addition, robots can be a great advantage for young surgeons with less experience performing operations that require a lot of experience for accuracy and precision [1].

Robotic surgery systems can be divided into haptic and autonomous types according to their degree of automation and dependence on the surgeon. While haptic (or tactile) systems grant the surgeon to guide the robot performance, autonomous robot systems can complete the routine by themselves after the surgeon finishes the plan and setup that the robot must follow [2]. Nonetheless, a robot-assisted orthopedic system requires a good pre-operative plan in which, by virtual modelling, a surgeon can implement his surgery strategy. In addition, the intraoperative image acquisition system is necessary to help the surgeon navigate in real time position. Furthermore, it is essential to do the matching between virtual data and the real position data within the operating room, being this process designated registration [1].

Moreover, orthopedic surgery has successfully introduced sophisticated computer-assisted methods and simulations. These new technologies enable a better and profound understanding of orthopedic pathologies through new techniques of computerized imaging and visualization tools that allow more precise and accurate measurements [3].

Femoroacetabular impingement (FAI) is a medical condition recognized as a cause of hip pain, cartilage or acetabular labral lesions and recently correlated with early osteoarthritis in adults. It is estimated to have a prevalence of 10-15% in the general adult population and is highly related to sports activity, especially its cam-type [4]. FAI can be considered a good applicant for robotic technology and computer-assisted methods due to its simple concept of mechanical collision of rigid bodies [3].

Preoperative planning is one of the essential prerequisites for the success of the orthopedic procedures [5]. Thus, the work presented in this thesis features a preoperative planning tool for conservative hip surgery assisted by a robotic system to correct the cam type FAI.

1.2. Objectives

The main purpose of this thesis is to develop a software using the MATLAB® and 3DSlicer image processing tools to help an orthopedic surgeon plan the surgical procedure to correct the patient's cam type femoroacetabular impingement condition.

The preoperative tool presented in this project was constructed in order to be part of robot-assisted conservative hip surgery procedure and it was assembled based on the MRI radial sequence acquired during diagnosis of patients with cam-type FAI.

The work developed and presented in this thesis can be divided into the following objectives:

- Geometric analysis of radial MRI from patients with cam-type FAI who underwent the traditional conservative hip surgery at Hospital da Luz;
- Femur segmentation;
- Creating an application in which the surgeon can delineate the region to operate in order to recreate the sphericity of the femoral head;
- Surface formulation that delimits the bone area to be removed during the surgical procedure that will act as the safety zone in which the robot arm is constrained to work;
- Registration between the formulated surface and the head of a plastic femur, which mimics the patient's coordinates in the operating room.

1.3. Thesis Outline

This dissertation is organized into five chapters: 'Introduction', 'Background', 'Image Processing', 'Results and Discussion' and 'Conclusion'.

First, chapter 'Introduction' presents the importance and objectives of this project.

Chapter 'Background' provides all the necessary information to prepare the reader to become familiar with the content of this thesis. Thus, the hip anatomy is presented, as well as the description of the medical condition addressed - Femoroacetabular Impingement - and the surgical procedure that will be innovated - Hip Arthroplasty. In addition, magnetic resonance imaging is described since it serves as the basis for formulating the preoperative planning tool. Finally, the state of the art is presented regarding surgical navigation, segmentation and registration, along with descriptions of recent examples in which robotic technology and computer-assisted surgery methods have been implemented to correct the FAI cam type.

Chapter 'Image Processing' accommodates all the methods implemented to formulate the software that enables the orthopedic surgeon to plan and delineate the region to operate, from geometric analysis of the radial MRI to the registration required between the preoperative planned surface and the real data on the simulated operating room.

Chapter ‘Results and Discussion’ presents the results achieved during this project and its analysis in relation to the defined objectives.

Lastly, chapter ‘Conclusion’ provides an overview of the developed work and its main results. In addition, some suggestions regarding future work are presented.

2. Background

2.1. Hip Joint Anatomy

The hip joint, shown in Figure 1, is the connective structure between the torso and lower limbs being the articulation between acetabulum of the pelvis and the femoral head. It is a ball and socket joint whose main objectives are stability and weight-bearing. It is considered a synovial joint since it has a joint cavity; articular cartilage covers the joint surfaces; synovial fluid is produced by the synovial membrane and is surrounded by a ligamentous capsule [6,7].

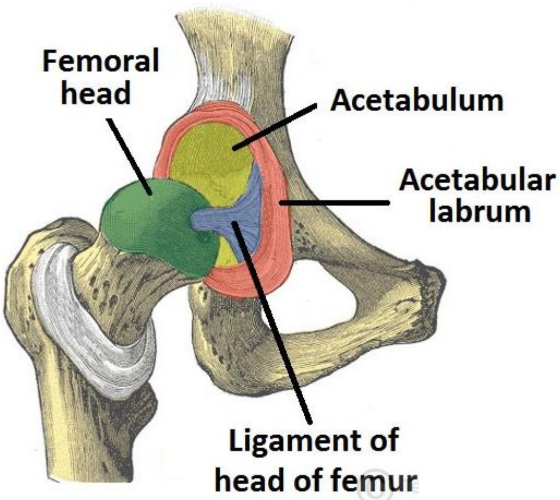

Figure 1 - Hip joint. (Image from [7])

In the inferolateral region of the pelvis there is a cup-shaped depression called acetabulum, and attached to its rim is the fibrocartilaginous labrum. The acetabular labrum contributes to the distribution of forces around the joint and the restriction of synovial fluid movement to the peripheral compartment of the hip. The femoral head fits completely into the concavity of the acetabulum, since it has a spherical format.

Articular cartilage covers both the acetabulum and femoral head, being thicker in the weight bearing areas. To accommodate the full range of motion, the articular cartilage should cover the femur head beyond the acetabular edge boundaries.

To increase stability, there are two groups of ligaments: intracapsular and extracapsular. The femoral head ligament is the only intracapsular ligament that bridges the acetabular fossa and the femoral fovea, as shown in Figure 1. Among the extracapsular ligaments, ilieofemoral, pubofemoral and ischiofemoral ligaments are the most important [7], represented in Figure 2.

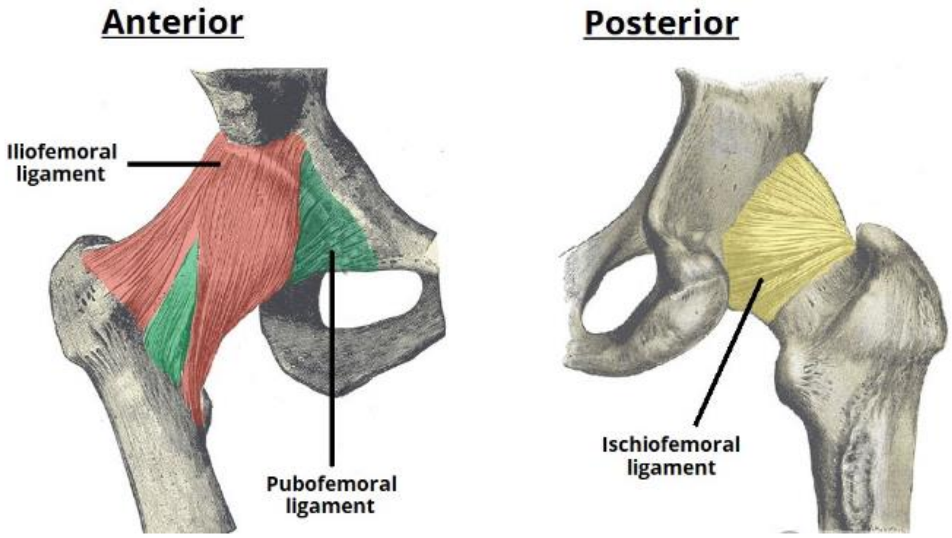

Figure 2 - Extracapsular ligaments in the hip joint. (Image from [7])

The iliofemoral ligament can be seen anterior to the hip in the form of an inverted 'Y' and runs from the anterior inferior iliac spine to a bifurcation in the intertrochanteric line of the femur. It prevents hyperextension of hip joint. The pubofemoral ligament has a triangular shape and arises from the superior pubic rami and inserts into the intertrochanteric line of the femur. It reinforces the anteroinferior portion of the capsule, preventing excessive abduction and extension. Posteriorly, the ischiofemoral ligament extends between the greater trochanter of the femur and the ischial body. It holds the head of the femur in the acetabulum with its spiral orientation, avoiding hyperextension.

Hip geometry permits a wide range of motion in all directions, such as flexion, extension, abduction, adduction, lateral rotation and medial rotation, where 22 muscles not only provide the necessary forces for these movements, but also ensure adequate stability [6,7].

2.2. Femoroacetabular Impingement

2.2.1. Definition

Femoroacetabular impingement (FAI) is a medical condition described as an abnormal contact between the acetabulum and the proximal femur in which there is a progressive joint damage and hip pain. It may be one of the leading causes of early osteoarthritis in adults [8].

This condition is characterized by a repetitive impingement on the interior of the hip joint during its motion, between the proximal femur at the head-neck junction and the acetabular rim, resulting in damage to the acetabular labrum and/or adjacent cartilage [9].

FAI can be classified into two different types: cam and pincer, even though there are many patients who have a combination of both.

Cam FAI can be described as abnormal morphology of the proximal femur, in which the femoral head loses its sphericity and the femoral head-neck offset decreases, as shown in Figure 3 – B). Femoral head-neck offset is defined in [9] as “distance between the widest diameter of the femoral head and most prominent part of the anterior femoral neck”. During hip flexion and internal rotation, the aspheric femoral head is forced into the anterosuperior acetabulum, which causes shear stress between cartilage and the labrum and also compression into the cartilage. Thus, patients with this type of impingement, have mostly chondral and labral lesions located anterosuperiorly.

On the other hand, pincer FAI is characterized with excessive acetabular coverage, as illustrated in Figure 3 – C). Here, the femoral head-neck junction contacts with the anterosuperior acetabulum rim, resulting in significant cartilage damage and labrum degeneration. In addition, in the posterior inferior portion of the joint subtle subluxation can occur.

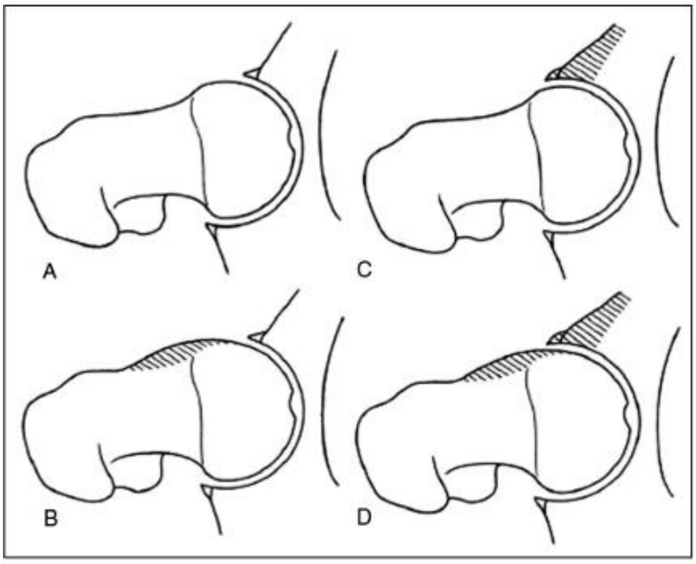

Figure 3 - Femoroacetabular impingement types. Diagram showing a healthy configuration of the hip joint (A), the aspherical femoral head in the cam-type deformity (B), excessive acetabular coverage in the pincer-type (C), and mixed cam and pincer (D). (Image from [9])

FAI syndrome is seen primarily in athletes, especially those who practice a sport that requires vigorous and repetitive hip flexion, internal rotation and adduction, for example, ice hockey, ballet or soccer. While cam-type is seen mainly in men ranging in age from 20 to 30 years, pincer-type is more frequent in middle-aged women [9].

FAI symptoms consist of recurrent groin pain, lateral trochanteric pain or both. The frequency of pain increases with degeneration of acetabular labrum and articular cartilage. There is evidence that some patients suffer from acute pain during physical activity which indicates a tear of the acetabular labrum. Usually, range of motion of the hip joint is limited and painful during flexion and internal rotation.

2.2.2. Diagnosis

To identify this condition, the physician can perform two physical exams: anterior impingement test, as showed in Figure 4 and log roll test. It is important that, during these maneuvers, the typical pain that patients experience during physical activity is recreated which advocate FAI. Also, it is crucial to check for coexisting disorders, such as lumbar spinal pathology or athletic pubalgia, compensatory disorders, like gluteal or abductor irritability or trochanteric bursistis or, even coincidental findings such as snapping hip. It is noteworthy that exists a high prevalence of FAI in the asymptomatic population [8].

Figure 4 – "Hip impingement test. The patient's hip is forcibly rotated internally, while in adduction and 90º of flexion. This maneuver approximates the anterolateral femoral head-neck junction with the anterosuperior acetabular rim, creating a shearing pressure on the acetabular labrum (or adjacent articular cartilage). A positive test produces anterior groin pain." (Image from [9])

To carefully evaluate the FAI condition, several imaging studies are performed. The diagnostic standard is a series of radiographs that include the anteroposterior pelvis centered on the pubic symphysis, lateral view of the proximal femur (which includes frog-lateral, 45°, and 90° Dunn lateral views) and a false profile view of acetabulum [8]. While the anteroposterior pelvic view allows visualization of the contour of the lateral femoral head-neck junction, in the frog-leg view it is possible to evaluate the anterior femoral head-neck offset [9].

Recently, magnetic resonance imaging (MRI) and MRI arthrography with gadolinium contrast (MRA) are preferred for a better assessment of FAI. MRI can easily detect joint effusion, labral pathologies and early cartilage changes, whereas MRA better visualizes joint surface anatomy and is more sensitive to labral pathology, but cannot detect effusion and is less sensitive to detection of subchondral changes [8].

In addition, computed tomography (CT) can be used to diagnose and plan the preoperative treatment of FAI and there are studies in which ultrasound can be an effective way to detect cam-type impingement, but it depends greatly on the experience and skill of the operator.

Typically, cam-type FAI is defined by the alpha angle with values above 55°, which can be quantified on radiographs and MRI by the angle formed between a line drawn along the femoral neck axis and a second line connecting the center of the femoral head to the anterior head-neck junction, as seen in Figure 5 [9,10].

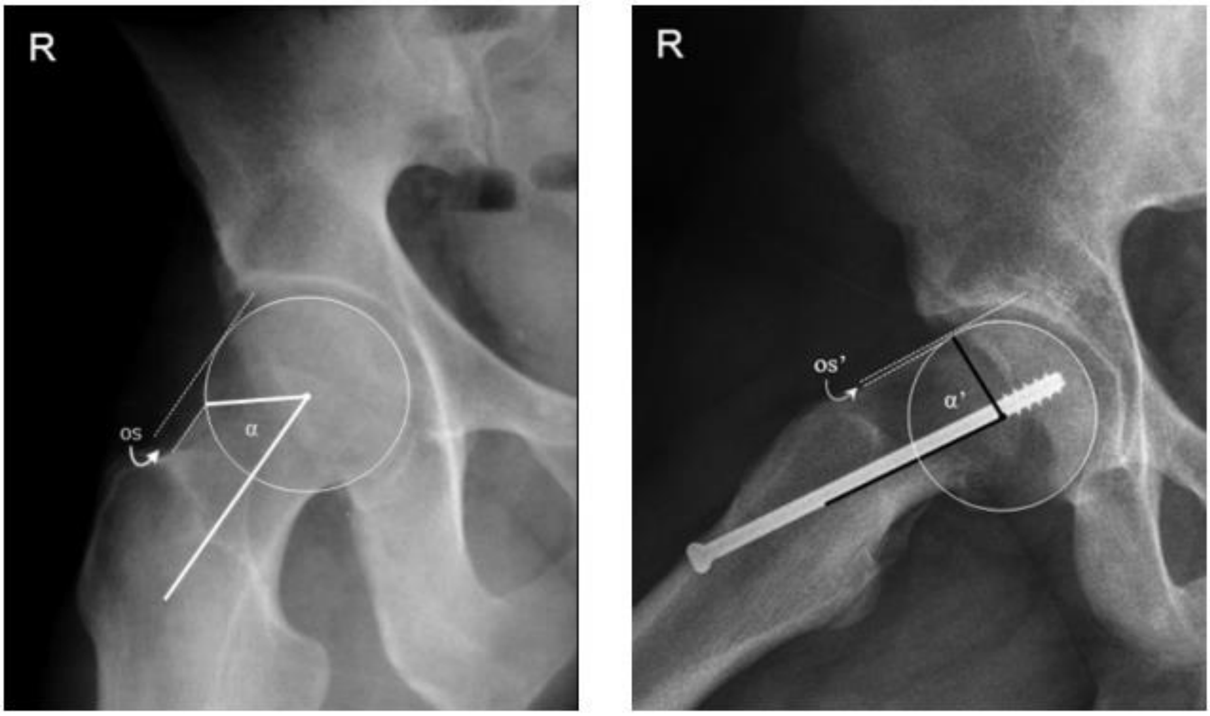

Figure 5 – Left Image: right frog-leg radiograph of a patient with normal anterior femoral head-neck junction (OS) and alpha angle (α). Right Image: right frog-leg radiograph of a cam-type FAI patient with a small anterior femoral head-neck offset (OS') and large alpha angle (α'). (Image from [9])

2.2.3. Treatment

Currently there are two treatment options: non-surgical and surgical methods.

Non-surgical treatment includes rest, activity modification, nonsteroidal anti-inflammatory drugs, physiotherapy and sometimes corticosteroid injections. This therapy may be effective in relieving acute pain, but it does not resolve the abnormal morphologies of FAI. In addition, symptomatic patients who delay their surgical correction may promote disease progression to the point where joint-preserving surgery can no longer be applied [9].

When patients with FAI present serious damage and considerable deformities, they need surgical treatment. Among adolescent athletes with FAI and labral tears who were treated with non-surgical methods, only less than 10% could avoid surgical intervention [8].

The aim of the surgical treatment is to alleviate the femoral impingement against acetabular rim, allowing for better and unobstructed hip motion. Both 'open' hip surgery and arthroscopy are good options for treating FAI, but the latter being less invasive is the best alternative with smaller incisions, shorter recovery times and lower morbidity rate, particularly for professional athletes [9]. After arthroscopy, most patients reached near normal or normal levels of functionality, returning to activity and sports [8]. On contrary, patients with advanced osteoarthritis undergo total hip replacement [9].

Unfortunately, there is a need for revision in failed surgeries due to residual deformities. Another rare complication is fracture of the femoral neck because of the excessive femoroplasty, reported in the adult population, with age being a risk factor [8].

2.3. Hip Arthroscopy

Hip arthroscopy is an increasingly performed procedure worldwide. As a surgical procedure, it requires perfect planning and technique for successful outcomes and is a procedure with a long learning curve [11,12].

Hip arthroscopy performed as a FAI treatment has been proven to be successful with pain relief and return to activities and sports. For this procedure, the ideal patient would be a 'young nonarthritic patient who is symptomatic and has clinical and radiologic evidence of focal impingement'. During this technique, the goals to be achieved are to reshape the femoral head to reach its spherical contour, normalize femoral offset, correct the acetabulum coverage, repair or rebuild both chondral and labrum damage to improve joint sealing and restore its normal mechanics [11].

To ensure a successful procedure, there are some crucial planning factors, such as patient positioning and setup, and the layout of the operating room (OR). During the surgery, the patient lies on the table with a large padded post between his legs in the supine position with both feet in the traction boots, as shown in Figure 6. Initially the hip is fully abducted and slightly flexed and only to the operative leg is traction applied. A C-arm x-ray machine is used to obtain adequate visualization of the anteroposterior pelvis and it must be positioned in a way it does not obstruct the arthroscopy screen.

Figure 6 - Patient positioning. (Image from [11])

Access to the hip joint is through two or three portals whose location is fundamental for instrumentation and visualization, as shown in Figure 7. The first one is settled with the help of x-ray in the anterior and superior region of the greater trochanter border and the others under direct view from inside the joint in a safe anterolateral zone of the thigh. During portal creation, the surgeon must be careful not to injure the labrum or femoral head cartilage. Afterwards, a capsulotomy is performed to improve the mobility of the arthroscopic instruments and to facilitate visualization in the peripheral compartment [11,12].

Figure 7 - At the beginning of the surgery, three portals were opened on the patient's hip. (Photograph taken during conservative hip surgery performed at Hospital da Luz on 04/04/2019)

The disease development dictates the next steps of the procedure, since not all patients need all of the following treatments. The acetabular cavity is first observed, where damage to the labrum and cartilage are repaired in the form of debridement, repair or reconstruction for tears and chondroplasty. In case of pincer impingement, during acetabuloplasty, the area of over coverage on the acetabular side is removed. During femoroplasty, for cam lesions, the femoral head and neck junction are reshaped into a normal sphere, as shown in Figure 8.

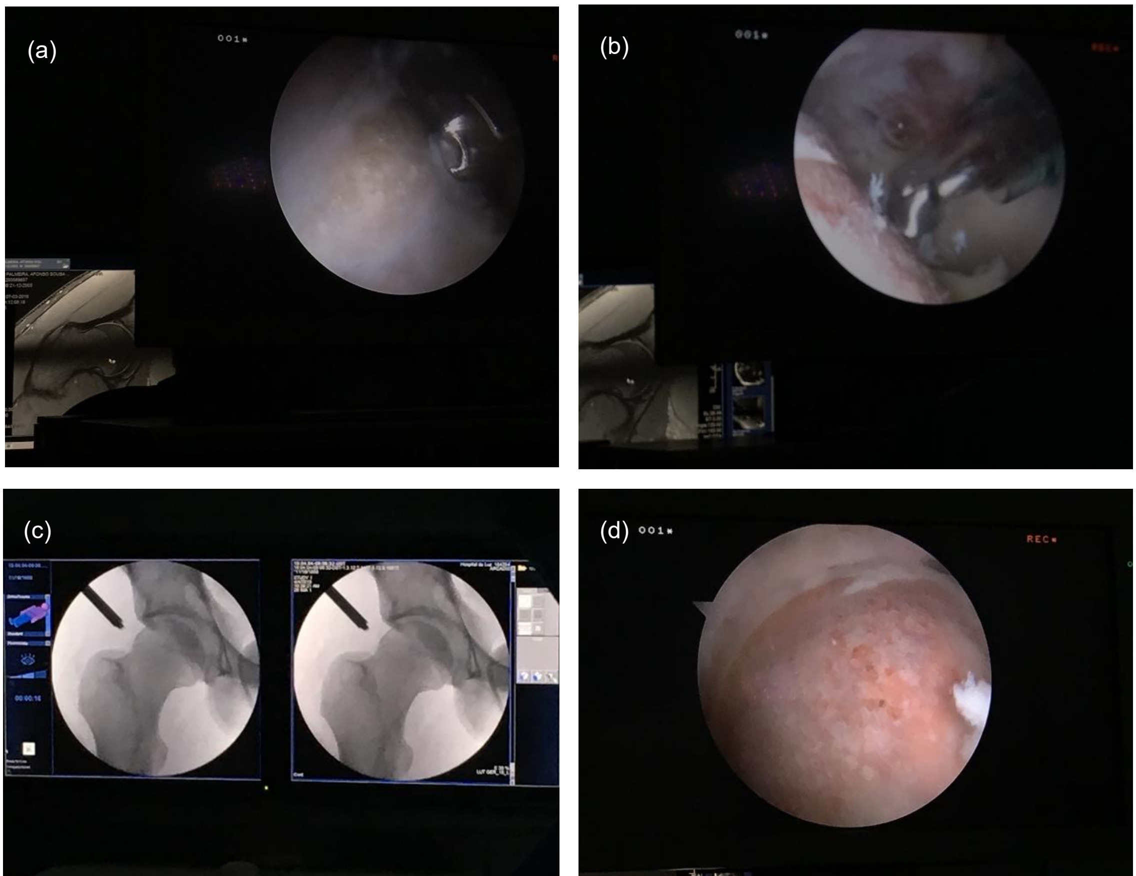

Figure 8 – Femoroplasty: (a) and (b) the surgeon drills the femoral head; (c) radiographs taken during surgery in which the surgeon can visualize the amount of bone still to be removed; (d) femoral head resulting after bone resection. (Photograph taken during conservative hip surgery performed at Hospital da Luz on 04/04/2019)

All bone resections are planned preoperatively, thus the C-arm is positioned so that its image closely matches the position on the preoperative scan, assisting in the orientation of the osteoplasty, avoiding complications. During femoroplasty, the leg is out of traction, so that it can be flexed, extended and rotated so the entire head-neck junction can be visualized in order to ensure adequate and no over-resection [11].

Finally, the large capsulotomy must be repaired, as shows Figure 9, and all portals must be closed. Throughout the surgery, it is required intensive irrigation to decrease the debris and the chance of heterotopic ossification. Also, this technique requires specialized tools of small dimensions.

Figure 9 - Surgeon repairs the capsulotomy. (Photograph taken during conservative hip surgery performed at Hospital da Luz on 04/04/2019)

Normally, hip arthroscopy allows for easy recovery with just one day of hospitalization and use of crutches for the first couple of weeks. Patients can easily return to their daily work, but sports should wait a few months [12].

Unfortunally, like any surgical procedures, there are complications associated with hip arthroscopy. However, most of them can be avoided by choosing the patient correctly and with meticulous planning, positioning and execution. The most common complications are nerve damage due to portal placement or traction and compression from positioning, which are often temporary and its prevention involves providing proper padding and respecting the time limits of traction. Moreover, at the onset of the learning curve, labral injury, cartilage scuffing and breakage of instruments are common. Sometimes chondral damage may occur due to careless instrument manipulation or poor anchor placement.

Revision surgeries may be required mainly because of deficient bone resection, due to poor visualization or planning, and lack of experience. While under resection can be treated with revision surgery, excessive resection leads to permanent damage to the hip joint. If, on the one hand, an overly aggressive rim trimming promotes hip instability with gross dislocation, on the other hand, over-resection on cam impingement leads to abnormal hip mechanics and possible fracture at the head-neck junction [11].

Thus, hip arthroscopy can be a successful treatment of FAI, as long as the surgeon has the necessary skills and the procedure is well planned and performed.

2.4. Magnetic Resonance Imaging

Magnetic Resonance Imaging, a spectroscopic imaging modality that uses non-ionizing radiation to create images of the interior of the human body, is commonly used as a diagnostic technique.

MRI is based on the principles of nuclear magnetic resonance (NMR), specifically in the absorption and emission of energy in the radio frequency (RF) range of the electromagnetic spectrum. The MRI signal arises from the interaction between the magnetic field and hydrogen nuclei, or protons. As the human body is composed mainly of water, the main source of hydrogen, it is possible to acquire a spatial map of the hydrogen nuclei in different tissues [13,14].

Briefly, a patient must lie down on an MRI scanner, a large and powerful magnet, and during the procedure a radio wave antenna send signals to the body and receives signals back. Attached to this scanner is a computer that converts the returned signals into images.

Exam time and its parameters depend not only on the scanner hardware and software used, but also on the anatomy portion being studied.

The process can be described into four parts: preparation, excitation, spatial encoding and signal acquisition.

1. Initially, a powerful and static magnetic field called B0 is produced by the magnet of the MR scanner. Naturally, the proton has an intrinsic magnetization designated spin, but when living tissues are placed in the presence of B0, the spin magnetization vector precesses around the magnetic field at a characteristic frequency, called Larmor frequency, proportional to the magnetic field intensity. Thus, all protons within the tissues become parallel aligned with the magnetic field.
2. Afterwards, a RF pulse is emitted from the scanner (its magnetic component is termed B1 field). It is called resonance, when the RF pulse is tuned to the Larmor frequency, which creates a phase coherence in the precession of all the proton spins. The spin magnetization is tilted perpendicularly to the magnetic field through a chosen RF pulse duration.
   Through Faraday induction, the transverse magnetization that still rotates as the Larmor precession, generates an electric current in the receiving coil, an electrical conductor, which is closed to the tissues. This NMR signal is attenuated due to relaxation processes after the RF pulse is switch off. The spin-lattice relaxation time – T1 corresponds to the time constant that the magnetization vector relaxes towards its equilibrium orientation that is parallel to the magnetic field B0 and the spin-spin relaxation time – T2 is referring to the loss of coherence of the spin system. The fact that different tissues have different T1 and T2 relaxation times leads to the contrast in MR images.

3. To perform spatial encoding, that is spins from protons in different locations do precess at slightly different rates, it is necessary to use magnetic field gradients, which are smaller additional magnetic fields that are turned on and off very quickly with an intensity that depends linearly on the spatial location.
4. The MRI signal is composed of the NMR signal obtained containing different frequencies corresponding to the different tissue spin positions after the use of gradient fields. After sampling, the analog MRI signal is digitized and processed by separating the signal contributions from different spatial locations representing different pixels in the final image through the Fourier transform [15].

An MRI sequence consists on the number of RF pulse and gradients which results in a set of images with a specific appearance. One way to classify the multitude of sequences available is according to the dominant influence on the appearance of tissues [16].

During hip joint examination, T1 weighted, T2 weighted, and proton density (PD) weighted are generally used. These three MRI sequences are characterized in Table 1. Moreover, all these MRI sequences are performed as turbo spin echo (TSE), which translates into reduced imaging time from the conventional spin echo acquisition technique, where repetition time and echo time are the two variables of interest.

Furthermore, there are different adjustments that can be performed in these MRI sequence. Fat suppressed (FS) imaging is a technique widely used when talking about hip joint imaging to suppress the signal from adipose tissue.

Table 1 - Characterization of diverse MRI sequences according to the tissue appearance, adapted from [10].

	White = high signal intensity	*Grey = intermediate signal intensity*	*Black = low signal intensity*
T1 weighted	Fat	Muscle	Fluid
T2 weighted	Fluid and fat	Muscle and brain grey matter	Brain white matter
Proton density weighted	Fluid and fat	Muscle and hyaline cartilage	Fibrocartilage

2.5. State of the Art

2.5.1. Surgical Navigation

In the field of orthopedics, there has been an increase in the use of robotic and image-guided technologies, as bones and periarticular soft tissues can be easily and accurately assessed using diagnostic technologies, such as radiography, fluoroscopy, computed tomography and magnetic resonance imaging. In addition, these types of tissues can be reconstructed into three-dimensional (3D) images, which allows simulations of preoperative surgical procedures. Furthermore, because bone is a hard tissue, it does not significantly deform as elastic tissues during surgery when it is cut or drilled, making it easier to apply preoperative imaging and planning information to surgery [17].

The objectives of using these new technologies are to improve accuracy in surgical procedures, facilitate minimum invasive surgery and explore new concepts in surgery. In addition, preoperative computational planning can be used to train and educate surgeons, as it allows the simulation of the procedure and the optimization of the surgical plan. During surgery, a visualization system is required to provide positional information about surgical instruments or implants in relation to a target organ. This is called surgical navigation.

Navigation systems are involved in three different types of surgical planning:

1. Volumetric image-based navigation, which, as its name implies, uses volumetric images like CT, MRI or ultrasound echography. The 3D image data can be presented in the multislice method, which is most commonly used to formulate an implant placement plan, because the computer-aided design files of implants are superimposed on the planes of the patient's anatomy. On the other hand, the 3D image of bones or implants may result from volume rendering or surface models. In this alternative method, there is the possibility of simulation of range of motion.
2. Fluoroscopic navigation where intraoperative fluoroscopic images are applied to construct the guiding map during the procedure. It requires a C-arm fluoroscope in the OR.
3. Imageless navigation depends on the kinetic information collected intraoperatively about joints or morphometric information in relation to target bones.

In orthopedics, most of the navigation systems use an optical sensor. This optical system normally involves charged coupled devices cameras based on infrared light to obtain the positional information. The infrared light is collected from a dynamic reference frame which is attached to the target bones and surgical tools to be tracked, with infrared light-emitting diodes or infrared light reflecting markers. These optical measurements are considered highly accurate and fast [17].

2.5.2. Segmentation

Bone segmentation is consider easier on CT due to its high resolution and high contrast between bone and surrounding soft tissues [17].

Nevertheless, B. R. Gomberg *et al.* [18] were able to develop a method optimized for detection of cortical boundaries in MRI images. The algorithm they feature started by defining the marrow region whose boundary was used to trace outward-directed test lines (which they called profiles) of sufficient length to transect the cortical bone, as shown in Figure 10 – a). They could detect the endosteal and periosteal boundaries through sequential profile maps using an intensity profile-based process, as illustrated in Figure 10 – b).

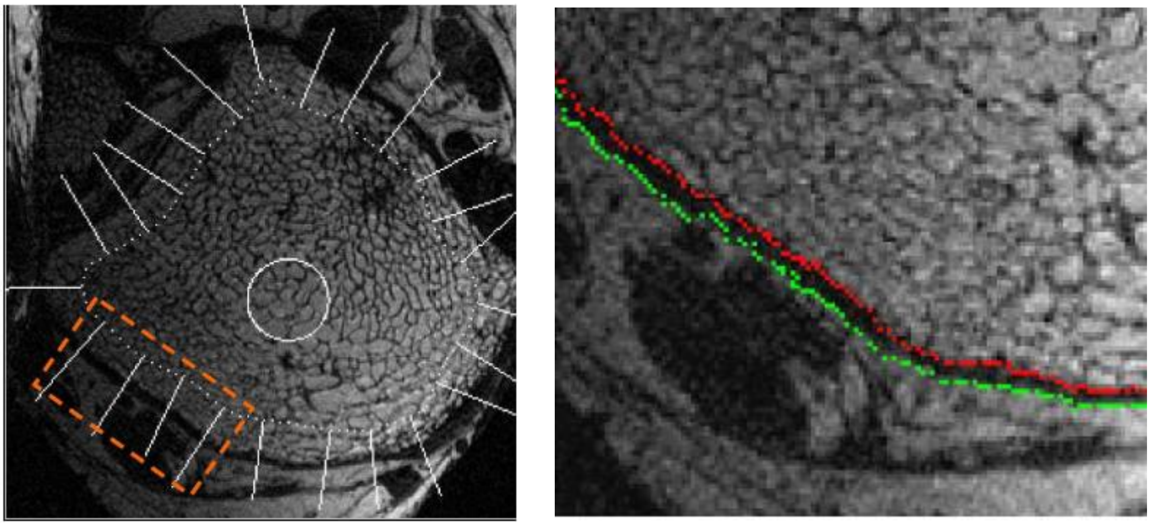

(a) (b)

Figure 10 - Cortical boundary detection algorithm: (a) marrow region where the dotted line represents the curve of points from which profiles are drawn outward and solid lines represent evenly spaced profiles along this curve, with each profile transecting the cortical shell; (b) endosteal(red) and periosteal(green) boundaries highlighted. (Image adapted from [18])

Moreover, H. Chen *et al.* [19] presented an automatic segmentation method of knee bone structures in proton density weighted contrast MRI sequence. The pipeline of their proposed method included 3D local intensity clustering-based level sets, inhomogeneity correction, generation of 2D intensity line image along the normal vectors of the rough surface, trabecular mask optimization and cortical mask detection. They compared their results with manual segmentation, as shown in Figure 11, where the final cortical mask within proposed method is yellow and manual segmented mask is green.

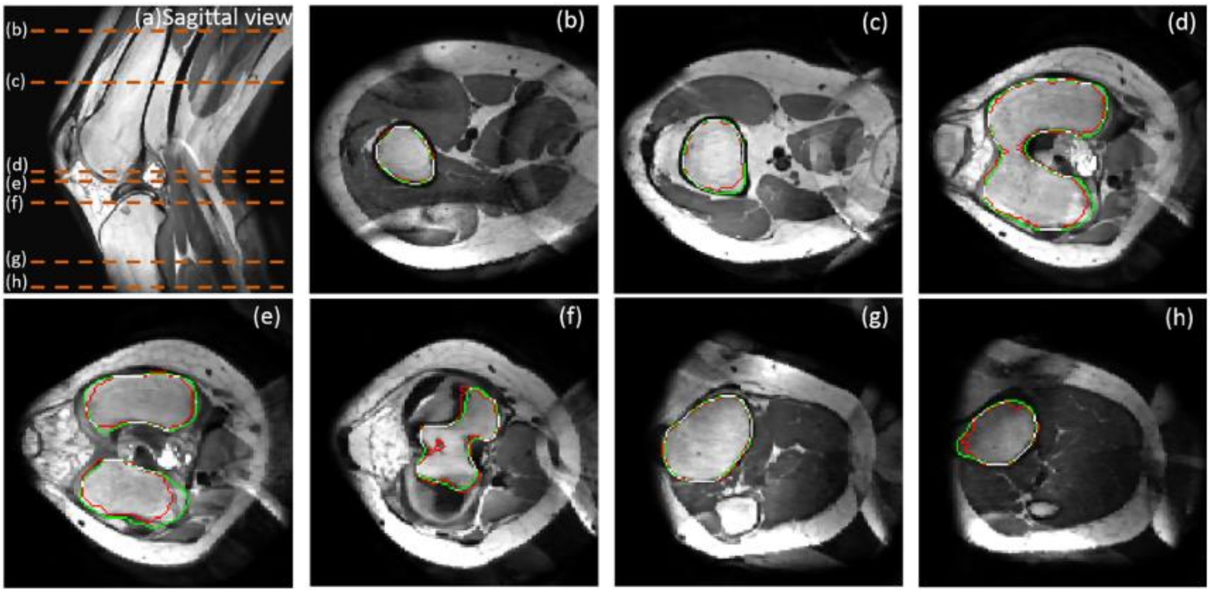

Figure 11 – (a) Sagittal view to show the position of the next images. (b)–(h)Transverse view with comparison results, where green contour is manual segmentation, yellow contour is cortical boundary of proposed method, blue contour is the initial cortical mask, red contour is the optimized trabecular mask and white points are the overlap between proposed method and manual segmentation. (Image from [19])

On the other hand, J. Schmid *et al.* [20] developed a semiautomated method for the segmentation of the proximal femur from radial MRI scans and reconstructed a 3D model, which can be used to plan hip preserving surgery. It included a random forest classifier and registration of a 3D template mesh of the femur to the radial images based on a physical deformable model, as Figure 12 explains.

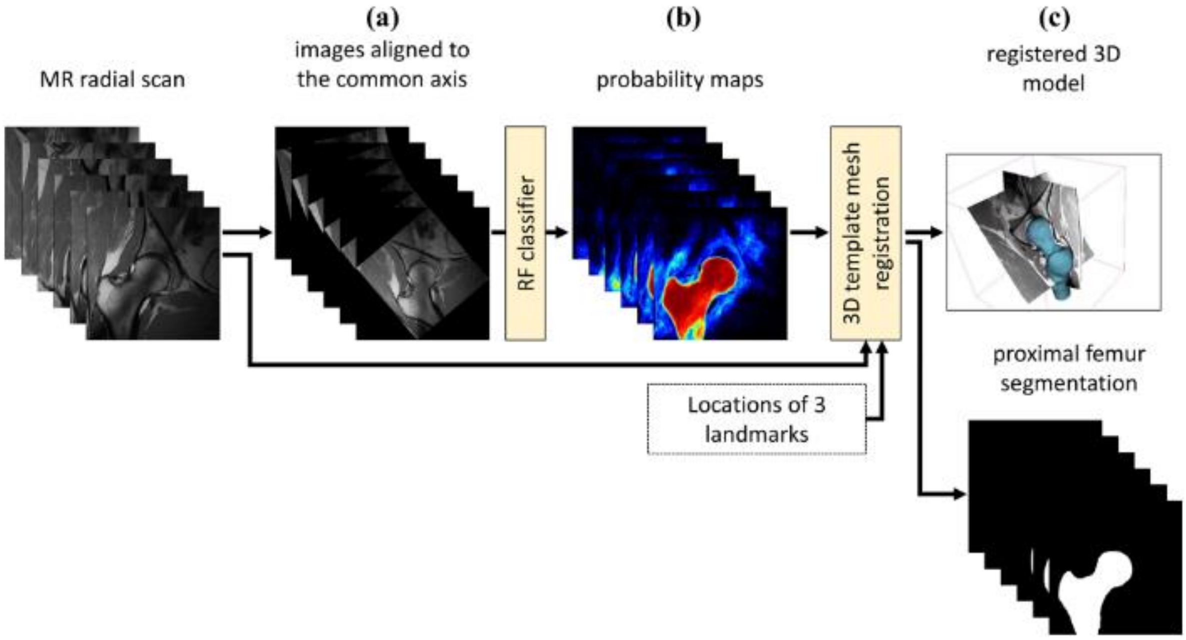

Figure 12 – Pipeline of J. Schmid et al. [20] work. "(a) The images of a radial scan are pre- processed, and they are aligned according the common axis of the scan; (b) the random forest classifier makes a prediction for every pixel of the images on whether it corresponds to femur. The generated probability maps are rotated back to the original orientations; (c) a 3D template mesh of the femur is registered to the radial images using the generated probability maps to drive the registration process and the positions of the three landmarks to initialize it." (Image from [20])

2.5.3. Registration

Registration is the mathematical relationship between the preoperative image coordinate system and the patient's intraoperative position data [17,21].

In orthopedic clinical applications, the use of rigid registration is more common and widely accepted, producing adequate results in surgical planning. In rigid registration, the transformation between two sets of points includes only linear conversions [22].

One method that can be implemented is called paired matching registration, in which the surgeon must identify three or more 3D landmarks on the patient during surgery, usually with a tracker, which correspond to landmarks previously collected on the preoperative images. Since this technique depends on the selection of registration points and the precise identification of corresponding point pairs that is susceptible to errors, artificial objects are implanted as fiducials to create an easy and exactly identifiable matching paired point. However, this method results in an additional operation to place the markers, which can bring discomfort and risk of infection to the patient.

Recently, an alternative method has been applied termed shape-based/surface registration. Here, several mathematical calculations are required, for example by applying the iterative closest-point algorithm and the least-squares method, to minimize the average distance between each intraoperatively measured point and the corresponding surface point of the computer model. The accuracy of the surface matching depends on the quality and quantity of intraoperative data sampling and on the accuracy of the computer models [17,21].

2.5.4. Computer-assisted surgery

Computer-assisted surgery is an advanced technique used for higher precision in performing surgeries. It involves a computer system responsible on 3D imaging for the purpose of preoperative planning and navigation assistance intraoperatively.

In orthopedics, it is mainly used in total joint arthroplasty in which the prosthetic joint is safer to be implanted accurately, or in the field of sports medicine, for instance reconstruction of the anterior cruciate ligament.

In recent times, computer-assisted hip arthroscopic surgery for FAI was presented by N. Kobayashi *et al.* [23]. It included three stages: preoperative evaluation, planning by virtual osteochondroplasty and intraoperative navigation assistance.

First, with the help of ZedHip software, the 3-dimensional model of the acetabulum and femoral head is built, from which it is possible to evaluate hip flexion through simulation and then perform a virtual osteochondroplasty in each axial computed tomography image, as shown in Figure 13.

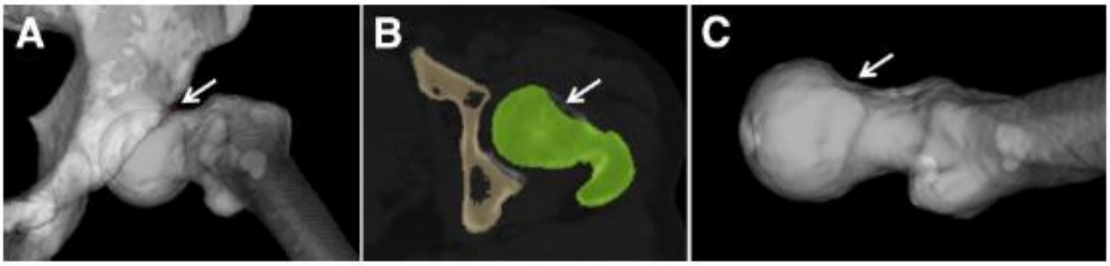

Figure 13 - (A) Impigement simulation; (B) virtual osteochondroplasty; (C) post-virtual osteochondroplasty. (Image from [23])

Thereafter, the planned 3D model is transferred to the navigation system and it is then necessary to perform point matching under fluoroscopic guidance and surface matching during the registration, as illustrated by Figure 14. Subsequently, the computer can monitor the resection area and depth in real time during the osteochondroplasty.

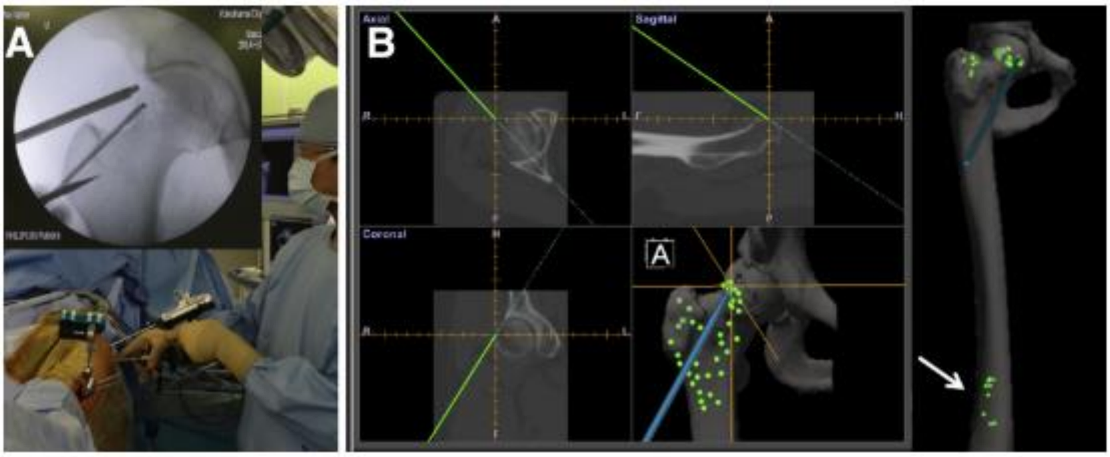

Figure 14 - (A) Point matching under fluoroscopic guidance; (B) surface matching during navigation system registration. (Image from [23])

The disadvantages inherent to this technique are radiation exposure by preoperative CT and during fluoroscopic matching and, also the tracker device requires an additional incision in the skin.

2.5.5. Robotic-Assisted Surgery

Robotic-assisted surgery is another intraoperative solution that improves surgical outcomes, increasing its accuracy. It involves an advanced surgical robot and depending on the type of surgery, the surgeon may or may not have a direct role during the procedure.

Tactile robotic-assistance is used in unicompartmental knee arthroplasty and total hip arthroplasty cup placement which present better results with better accuracy when compared to conventional techniques.

It has recently been shown by C. N. Park *et al.* [24] that robotic-assisted femoral osteochondroplasty is more accurate than a conventional technique for the treatment of cam-type FAI. This indicates that robotic-assistance may reduce the number of revision hip arthroscopies that are performed to re-reshape the femoral head junction.

The surgeon can create a preoperative plan through the 3D computerized model generated by the CT scans, as exemplified in Figure 15. Afterwards, intraoperatively during osseous resection, a robotic arm can guide the surgeon providing visual and haptic feedback. The main advantage of this system is that the robot limits the movements of the surgeon within the confines of the predetermined resection zone.

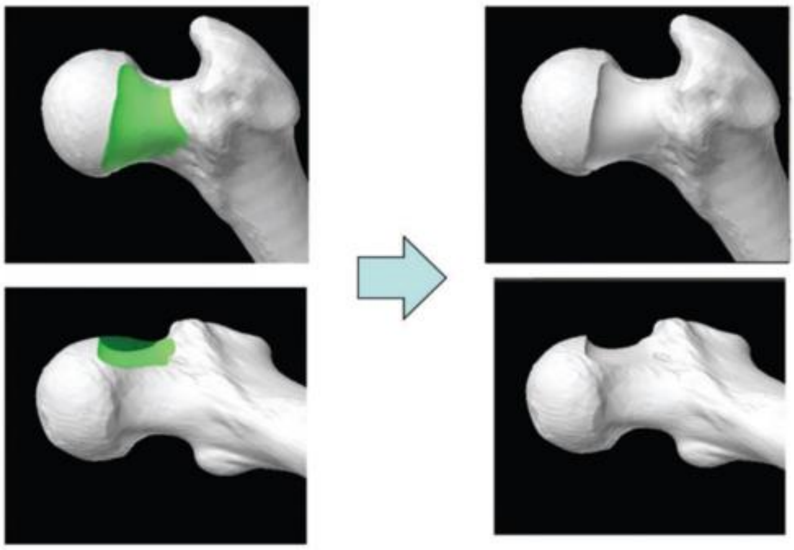

Figure 15 – Ideal final resected shape model generated by the preoperatively planned desired resection volume. (Image from [24])

In this study, they used a MAKO Robotic-arm Interactive Orthopedic System which consists of a robotic arm, an optical infrared camera and a user interface module. After generation of a 3D haptic resection volume, this volume information was saved into the system to allow the definition of the resection boundaries that were visible during the procedure. In the intraoperative, the surgeon receives from the robot visual and tactile feedback of resected bone, and also haptic feedback through its stiffness when excessive pressure or rapid movement are applied. If the surgeon unintentionally tries to resect bone out of the planned preoperative volume, the robot stops the cutting instrument immediately.

Another finding in this study was that robotic-assistance surgeries were significantly faster during bone resection than the freehand technique because there was no need to spend time carefully contouring the femoral head-to-neck junction since the robot induces a haptic barrier in the planned resection zone.

In an earlier study by M. Masjedi *et al.* [25], the use of robotic technology during the corrective surgery of cam-type FAI was validated. Here, the Acrobot Sculptor robot present in Figure 16 was used which restricted the movement of the surgeon’s cutting burr.

Figure 16 - Acrobot Sculptor Robot. (Image from [25])

Three-dimensional plastic models were constructed from a set of CT scans of three patients and then they performed a 3D surgical plan using a custom written software in C++ that needs to be imported into the robot. They fit a best sphere for the femoral head and also a hyperboloid to normal posterior and inferior region of the three femurs to be used as a constraint. This robot has a tracking arm which is secured to the bone with bone pins, and a sculpting arm with the burr tip. Both arms must be calibrated before procedure and then the surface models of bones were registered to the physical models by collecting a series of points. During bone resection, the surgeon has visual feedback from a screen in real time.

To evaluate the use of robotic technology in this type of surgery, it was quantified the reduction of 3D alpha angle taken from 360° around the femur neck using 3-Matics software and a custom written algorithm in MATLAB®. It was also evaluated prior and post-resection the 3D neck head ratio calculating four distance points along the femur neck.

In this study, it was successfully validated that with this robotic technology, under-resection and over-resection of femoral cam deformities were prevented.

3. Image Processing

This chapter presents all the methods implemented throughout the project, from comparing the radial and parallel MRI sequences to the graphical user interface (GUI), which allows the orthopedic surgeon to plan and delineate the region to be operated and the registration required between the preoperative planned surface and the real data on the simulated operating room.

3.1. MRI Radial vs Parallel

Normally, when talking about magnetic resonance imaging, one thinks of parallel slices at orthogonal anatomic planes. These are taken perpendicularly to important anatomic structures which are directed with the sagittal, axial or coronal planes. Furthermore, there exists the possibility to get oblique parallel slices relative to these planes to follow some leaning orientation arrangement.

When referring to the hip MRI, a patient in supine position performs several sequences at the hips with 15° internal rotation, where it is used tape in his toes to maintain his position [26].

At Hospital da Luz, to evaluate femoroacetabular impingement, the following sequences are performed:

- Axial T1 → T1_tse_axial
- Axial DP-FS → DP-FS_tse_axial
- Coronal DP → DP_tse_coronal
- Coronal DP-FS → DP-FS_tse_coronal
- Sagittal DP-FS of the femoral neck → DP-FS_tse_sag_neck
- Sagittal DP-FS of the acetabulum → DP-FS_tse_sag_acetabulum
- Axial T2-FS both hips → T2_tse_FS for both of the hips [27]

Unfortunately, the hip joint has a particular anatomy which complicates its imaging in conventional imaging planes. Because of its spherical shape, abducted and anteverted orientation, pathologies associated with the articular cartilage and the acetabular labrum have been studied using radial sections. These are acquired perpendicular to the surfaces of the hip joint, centered on a planned radial axis, providing a cross section of the labrum and articular cartilage with a full visualization of the entire acetabular circumference [28,29].

Therefore, in addition to the conventional imaging planes, the following two radial sequences are also performed: DP and DP-FS weighted → Radial_DP and Radial_DP-FS [27].

Qualitatively, radial images grant more detailed information respecting the labrum and cartilage when compared directly with the conventional planes: sagittal, coronal or axial.

With these last sequences applied to the hip joint, disproportional sections are produced in which acetabular cartilage, labrum, femoral cartilage and femoral head acquire different proportions due to the nearly spherical shape and oblique anatomic position of the hip joint, as analogous exemplified with an orange in Figure 17.

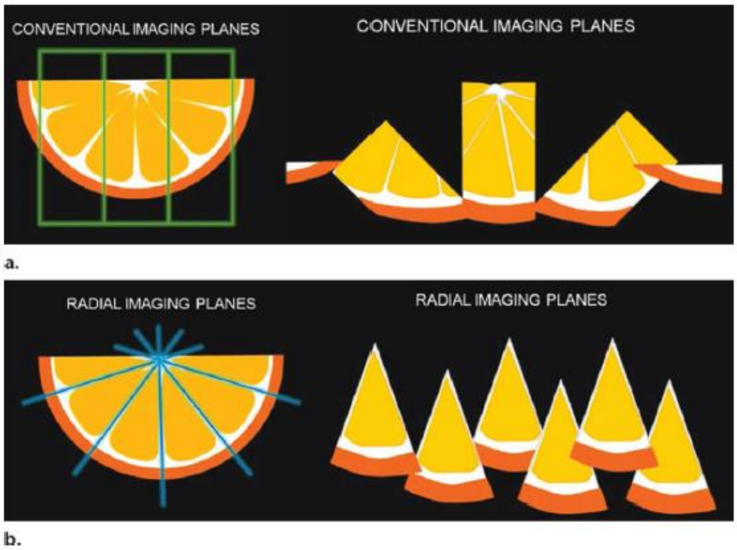

Figure 17 – Comparison of conventional (a) and radial (b) imaging planes. (Image from [28])

This disproportionality is reflected in the partial-volume-averaging effects in which in adjacent regions of a curved surface a voxel contains sudden changes of tissues that cannot be represented accurately. This problem mostly affects the antero- and posterosuperior regions of the hip joint in axial and coronal plane and, also, the superior region in the sagittal plane, as shown in Figure 18.

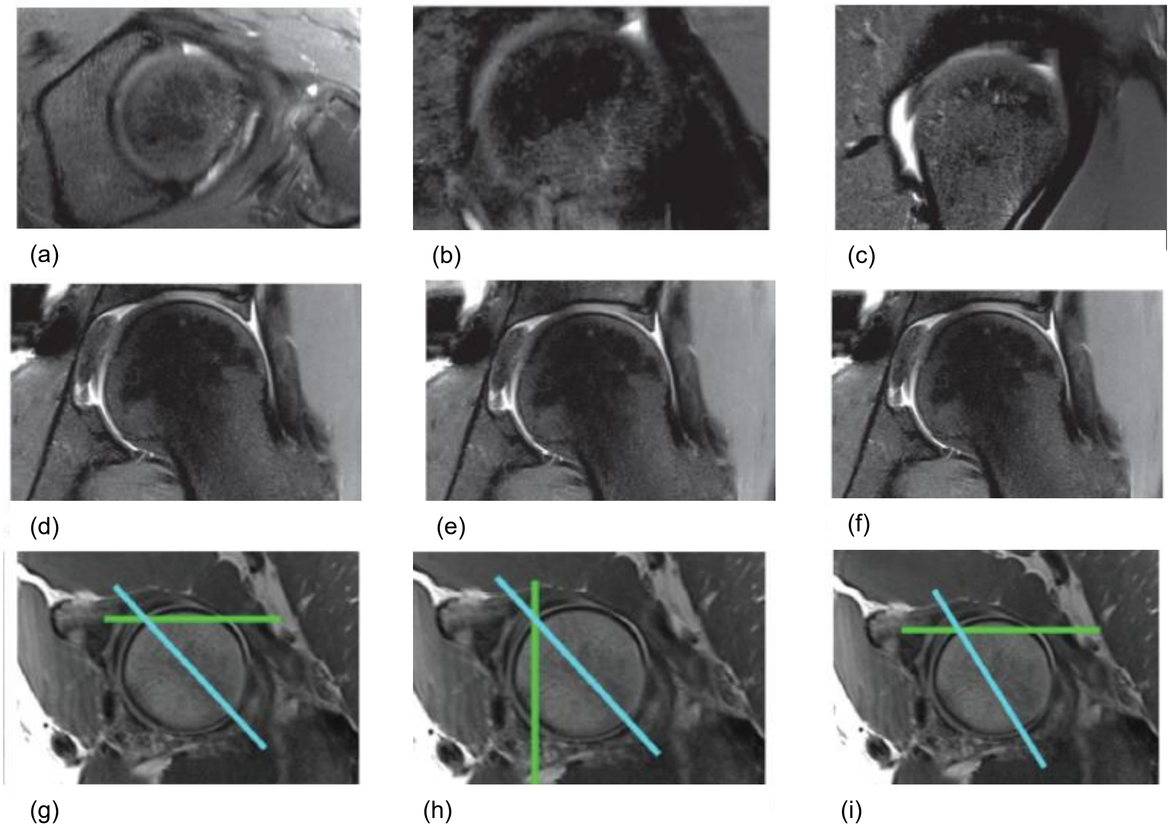

Figure 18 - Comparison of conventional slices (a – axial oblique; b – coronal; c – sagittal) and radial (d-f) imaging planes. The MR images obtained at the level of the acetabular opening (g-i) show the location of conventional slices (green line) and radial slices (blue line). (Image from [28])

Moreover, to ensure the optimal image of the labrum, the radial images must be obtained perpendicularly to the acetabular opening due to its anteverted position in the transverse plane and its inclined position in the coronal plane, as represented in Figure 19.

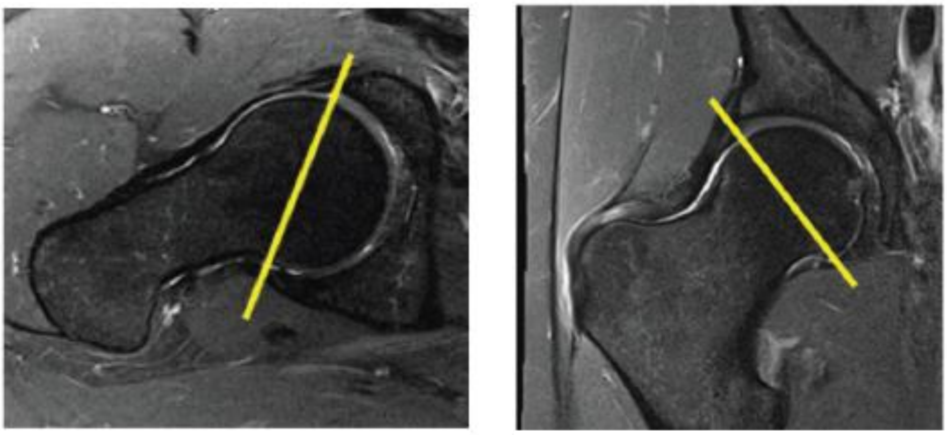

(a) (b)

Figure 19 - Radial MR images show that the acetabular opening is anteverted (yellow line in a) and inclined (yellow line in b). (Image from [28])

Furthermore, the radial sequences are the last to be performed, since they require a positioning process, using the sagittal image of the acetabulum and the coronal view of the femoral neck as reference. At Hospital da Luz, the standard procedure includes the collection of 24 slices, one every 7.5°, as represented in Figure 20, which result in 48 images after post-processing [27].

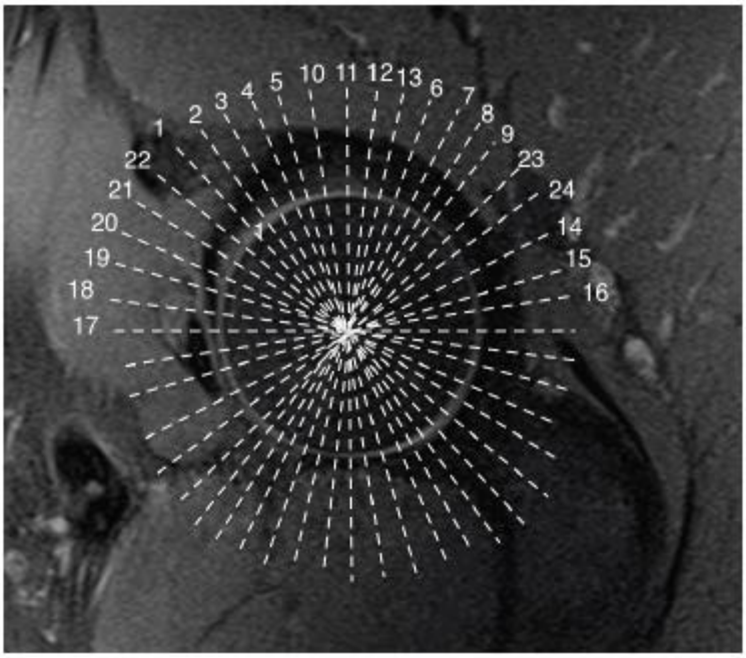

Figure 20 - MRI sagittal view of the maximum acetabular circumference showing the 24 radial slices acquired in no particular order (the MRI scan chooses the scanning order). (Image from [27])

The radial scan performed is considered a multislice sequence, which in one hand it takes a short scan time and allow a high resolution matrix to be scanned, on the other hand it produces a specific artifact in the image called crosstalk which appears in line with the radial axis, as one can see in Figure 21. Since this type of sequence is used to evaluate the acetabular labrum region, this artifact does not interfere with that visualization [29]. The crosstalk artifact is caused by interference in adjacent images that consequently produce a low-signal-intensity bar-shaped area overlaying the femoral neck. That is, if all radial imaging planes go through the center of the joint, after the first image is obtained, each successive image will include spins that have already been partially saturated, which affects the contrast in the center of the field of view of each image. The artifact's width depends on the angle between slices, meaning that the artifact will be wider when the angle between sections is smaller [28].

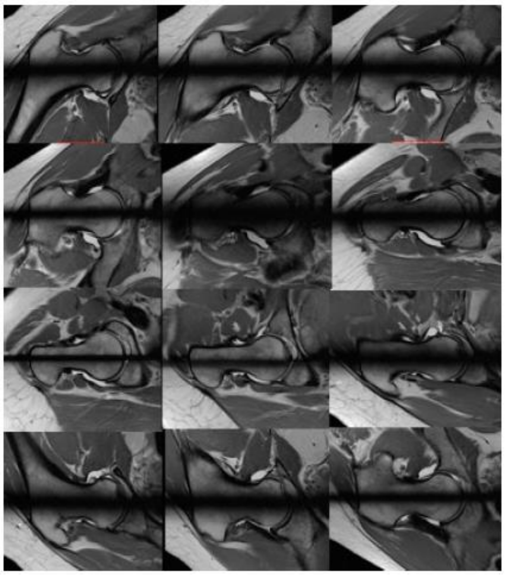

Figure 21 - MR radial sequence evidencing the crosstalk artifact. (Image from [27])

In quantitative terms each radial slice is a matrix of 384x384, in which there is 0.42mm of pixel spacing. A MATLAB® Bridge Extension was created in 3D Slicer, where a 3D volume was reconstructed based on all 48 radial images. For that, the MATLAB®'s interpolation function *scatteredInterpolant* was used and the linear interpolation method was chosen due to the long computational time it took to run higher order interpolation methods. The resulting volume of 178x231x231 has a voxel spacing of 1mm. In 3D Slicer, it is possible to obtain the visualization of axial, sagittal and coronal views of this volume, as shown in Figure 22.

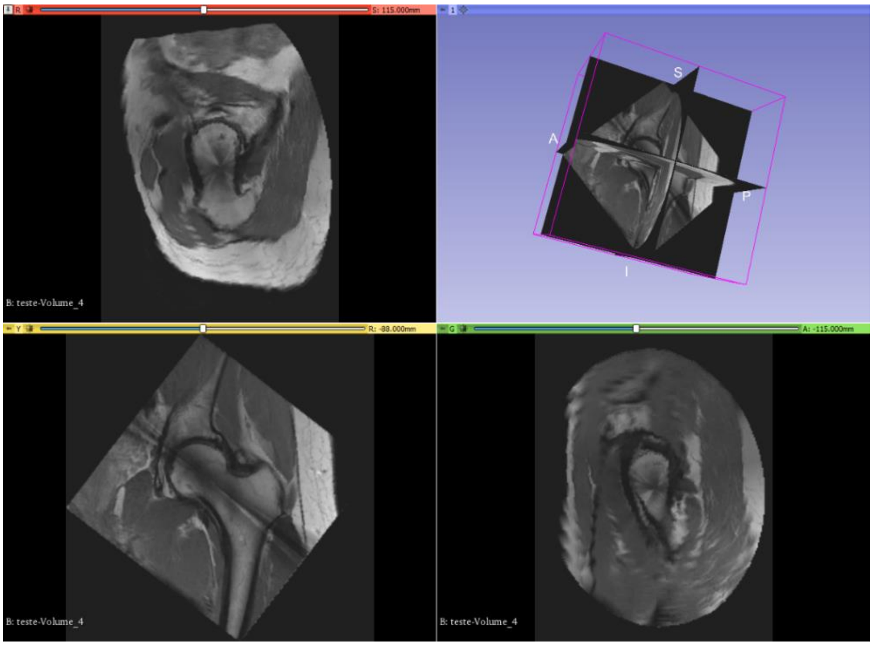

Figure 22 - 3D Slicer view of the interpolated volume.

Comparing these values, one can conclude that even though each radial slice has a better resolution than the interpolated volume, between each radial slice there is missing information in space, specifically when further from the center, as shown in Figure 23. Thus, this interpolated volume has a tradeoff between having information away from the radial axis, but with a worse resolution than at its center.

In orthopedics, having a volume of these dimensions with a millimeter error of magnitude is considered satisfactory for the current problem.

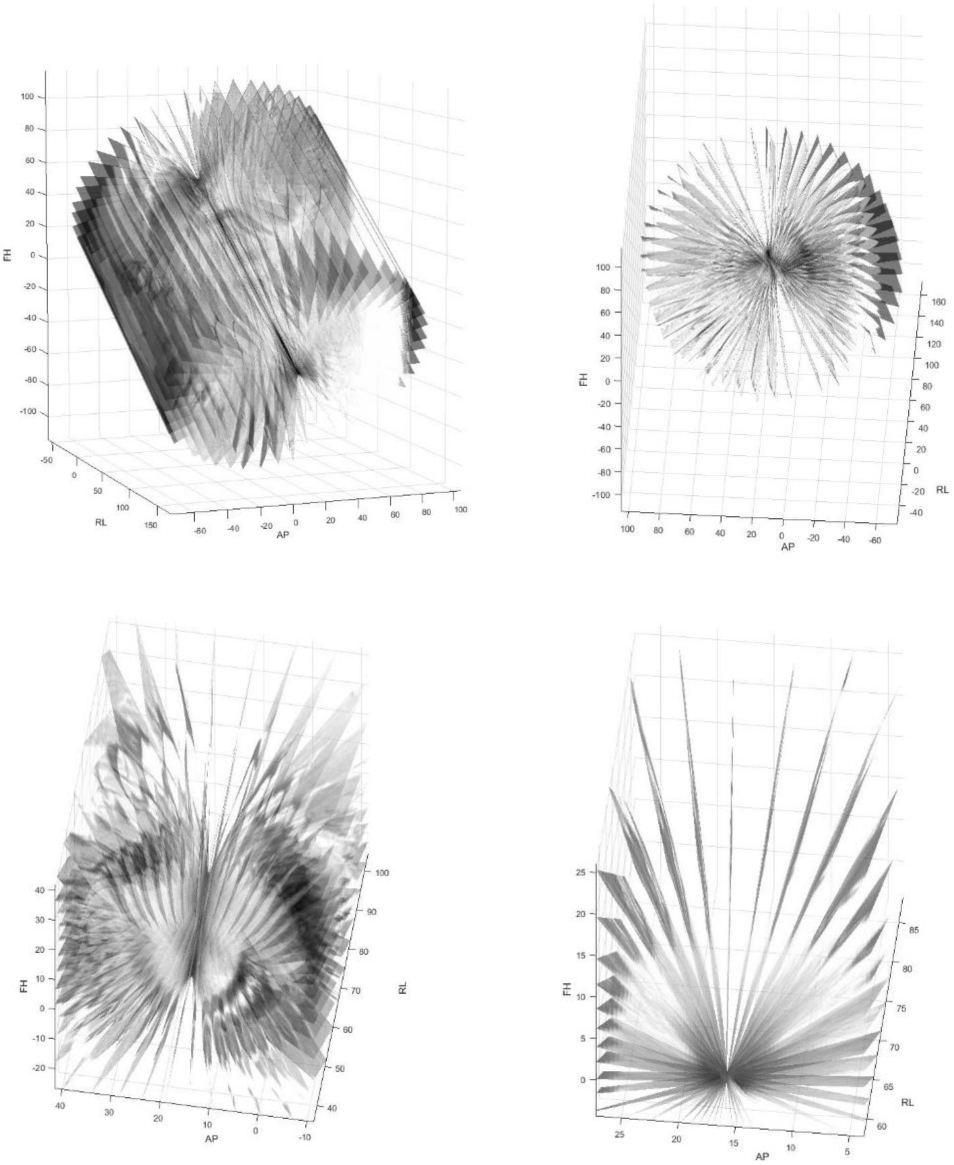

Figure 23 – MRI Radial sequence in 3D space from different points of view.

3.2. DICOM files

Each MRI slice used in this work is saved in Digital Imaging and Communications in Medicine (DICOM) format.

DICOM files are a universal data standard for storing, viewing and processing medical images, produced by a wide variety of radiological hardware. Not only DICOM files store the medical image data, but they also contain detailed metadata about patient information [30,31].

In other words, each DICOM file contains the medical image intensity values and different aspects of the patient, from personal characteristics such as name, gender and age, to the coordinate system, such as image position and orientation in relation to the patient's anatomy. Each information is encoded in an attribute in the form of a tag that includes the group and element numbers of the DICOM format. Table 2 displays the attributes used along this work and their description [32].

Table 2 - DICOM attributes.(Adapted from [32,33])

Name	Tag	Description
Image Position (Patient)	(0020,0032)	Coordinates (x,y,z) of the upper left corner of the slice with respect to the patient anatomy coordinate system.
Image Orientation (Patient)	(0020,0037)	Direction cosines of the first row and the first column of the slice with respect to the patient anatomy coordinate system.
Pixel Spacing	(0028,0030)	Numeric pair that corresponds to the physical distance in mm between the center of each pixel between adjacent row and adjacent columns.
Columns	(0028,0011)	Number of columns in the image.
Rows	(0028,0010)	Number of rows in the image.

Knowing the position and orientation of each slice and its dimensions, it is possible to visualize in 3D space each MRI scan using these attributes. By stacking all the slices in space, it is possible to perceive the volume of the patient's region of interest.

The reference coordinate system (RCS) of the DICOM files is the LPS coordinate system, in which the x-axis goes from right to left (L axis), the y-axis goes from the anterior region to the posterior region (P axis) and the z axis goes from inferior region to superior region (S axis). The image coordinate system of each MRI slice is defined regarding to the patient anatomy coordinate system. [32]

Using the attributes relative to the image plane and pixel spacing, it is possible to position and orient each MRI slice regarding to the patient coordinate system [33], as illustrated by Figure 24. The mapping of pixel location (i,j) to the RCS is given by:

$$\begin{bmatrix} x \\ y \\ z \end{bmatrix} = \begin{bmatrix} x_0 \\ y_0 \\ z_0 \end{bmatrix} + \begin{bmatrix} aR_1 & bC_1 \\ aR_2 & bC_2 \\ aR_3 & bC_3 \end{bmatrix} \begin{bmatrix} i \\ j \end{bmatrix} \tag{1}$$

where:

- (x,y,z) are the spatial coordinates of the pixel in the frame's image plane in mm;
- (x_0,y_0,z_0) are the three values of the Image Position (Patient) attribute which corresponds to the location in mm from the origin of the RCS;
- *a* represents the column pixel resolution given by the first number of Pixel Spacing attribute in mm;
- *b* corresponds to the row pixel resolution given by the second number of Pixel Spacing attribute in mm;
- (R_1,R_2,R_3) are the three values from the row direction cosine of Image Orientation (Patient) attribute;
- (C_1,C_2,C_3) are the three values from the column direction cosine of Image Orientation (Patient) attribute.
- *i* is the column index to the image plane;
- *j* is the row index to the image plane.

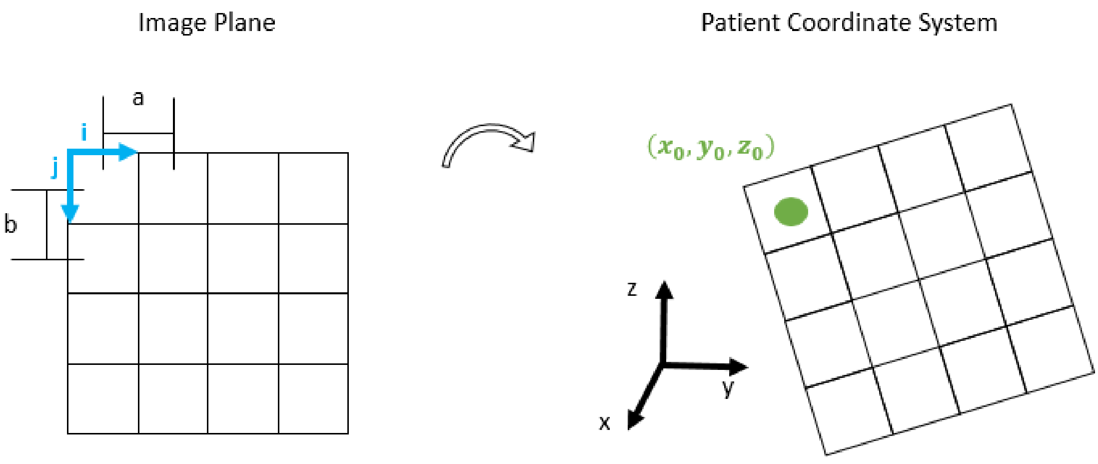

Figure 24 - Mapping of pixels into the patient coordinate system.

3.3. Segmentation

In the MRI radial sequence, the gray scale has different tones due to differences in the composition of each tissue. In the femur there are two types of osseous tissue: cortical and trabecular bone, which have reversed shades, as shown in Figure 25.

In addition, magnetic resonance imaging has intensity inhomogeneities because of coil sensitivity and B1 inhomogeneity, which cause a slow varying intensity gradient seen in brightness differences in each slice. Also, among the structures of interest there is a problem of low contrast, for instance, between cortical bone and ligament, as also seen in H. Chen *et al.* [19] work.

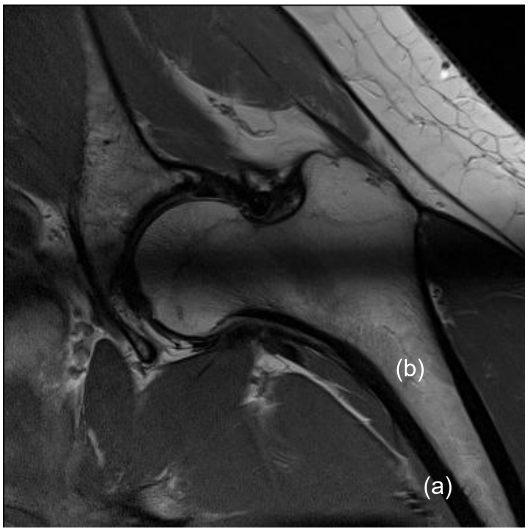

Figure 25 - Slice of radial sequence in which it is possible to observe the differences between cortical (a) and trabecular (b) bone.

3D Slicer has several tools to perform segmentations within the 'Segment Editor' module. With the volume uploaded and using the 'threshold' tool, it was not possible to distinguish the femur from among all the other structures present, as demonstrated in Figure 26 in which was used the Otsu Threshold option.

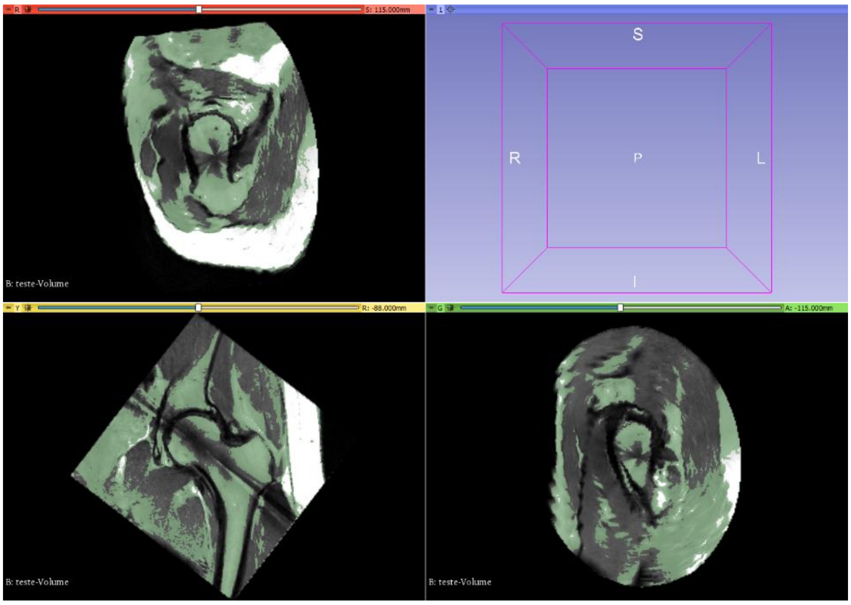

Figure 26 - 3D Slicer view when using segment editor Otsu Threshold tool.

To overcome this problem, the method 'grow from seeds' available in 3D Slicer was attempted. This consisted on drawing inside the femur several segments that constitute the 'seeds' from where the algorithm begins to grow until it reaches the segmentation. Unfortunately, for the current volume, only the trabecular bone was segmented and the resulting surface was not smooth due to the interpolation performed before, as illustrated in Figure 27.

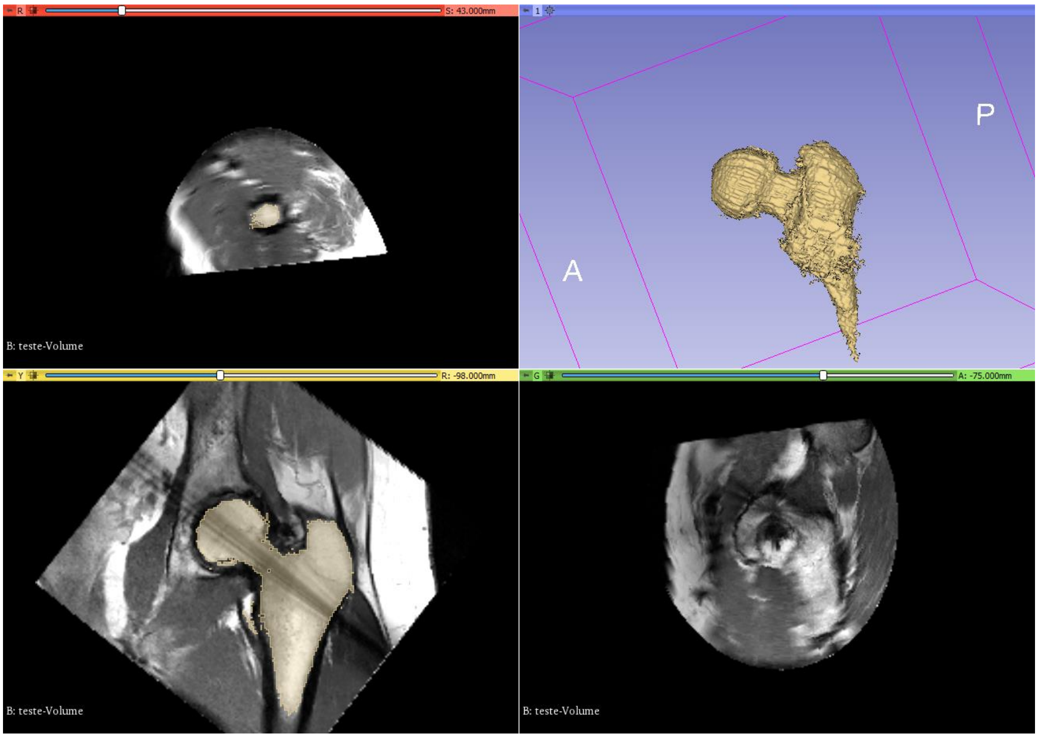

Figure 27 - 3D Slicer view from the trabecular volume segmented after using 'Grow from seeds' tool in Segment Editor.

Since the structures around the femur were part of the obstacles encountered in 3D Slicer, the strategy changed in order to first segment the femur within each two-dimensional (2D) radial slice before its transformation in a 3D volume.

In MATLAB®, several segmentations algorithms conventionally used in MRI were performed, but none of them could overcome the crosstalk artifact issue, as demonstrated in Figure 28.

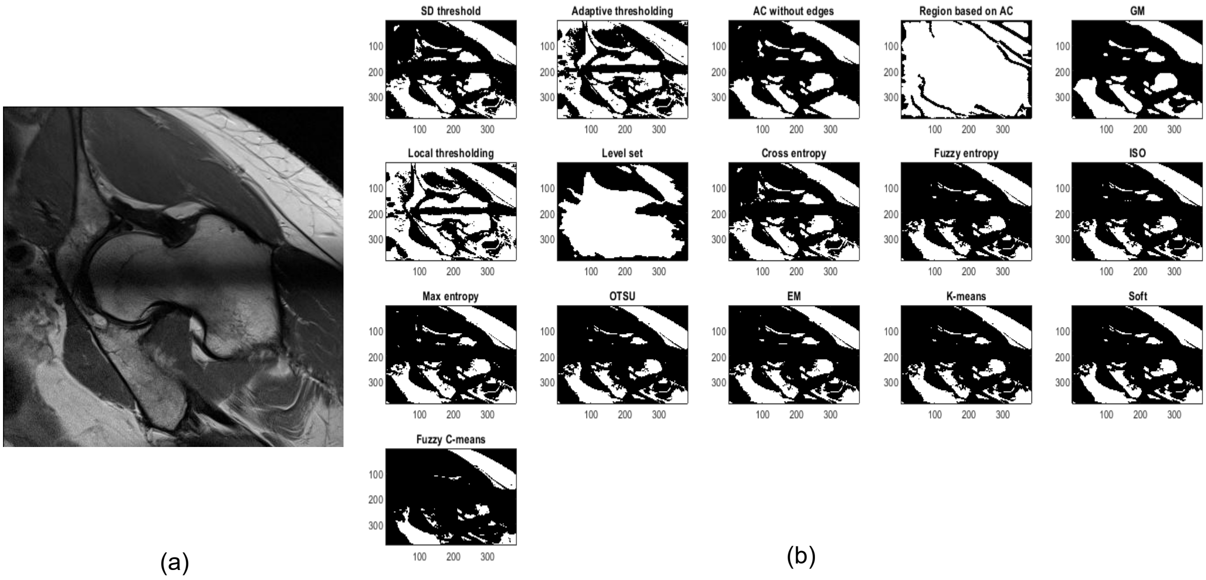

Figure 28 – (a) Original radial 2D MRI scan. (b) Different MATLAB® segmentations algorithms.

Based on the study of J. Schmid *et al.* [20], a different and innovative pipeline was followed, in which there is a pre-processing step where a 'pixel classifier' algorithm would be trained and then would classify and segment each of the radial 2D MRI scans.

First, the model was trained based on two classes, that were the manual segmentation of both cortical and trabecular bone of seven different images of the radial sequence, chosen based on their particular femur position. Figure 29 illustrates the manual segmentations performed at three of the radial slices chosen to constitute the training data.

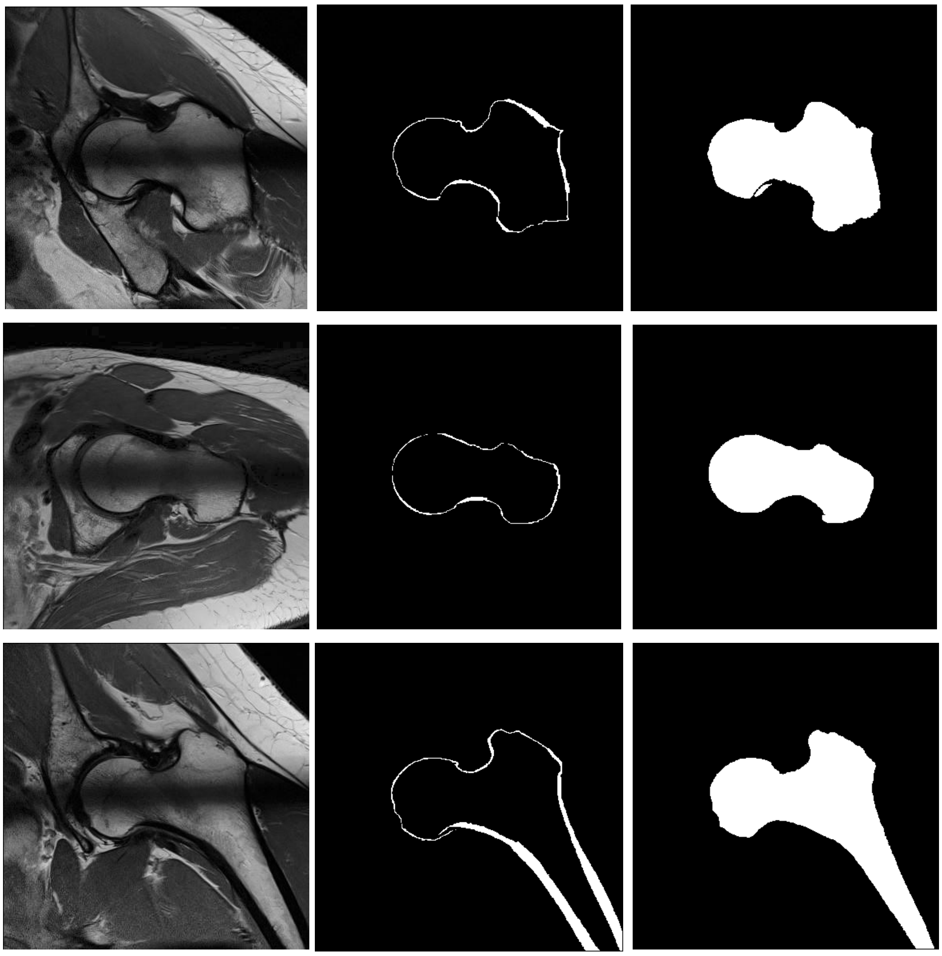

Figure 29 - Three examples of the data train: first column corresponds to the original slices from the radial sequence, second column is the manual segmentation of the cortical bone (1st class) and third column corresponds to the manual segmentation of the trabecular bone (2nd class).

After the model is trained, all 48 images belonging to the radial sequence were processed, resulting in a 2D radial sequence in which the crosstalk artifact was almost removed, as exemplified in Figure 30 by one of the radial slices.

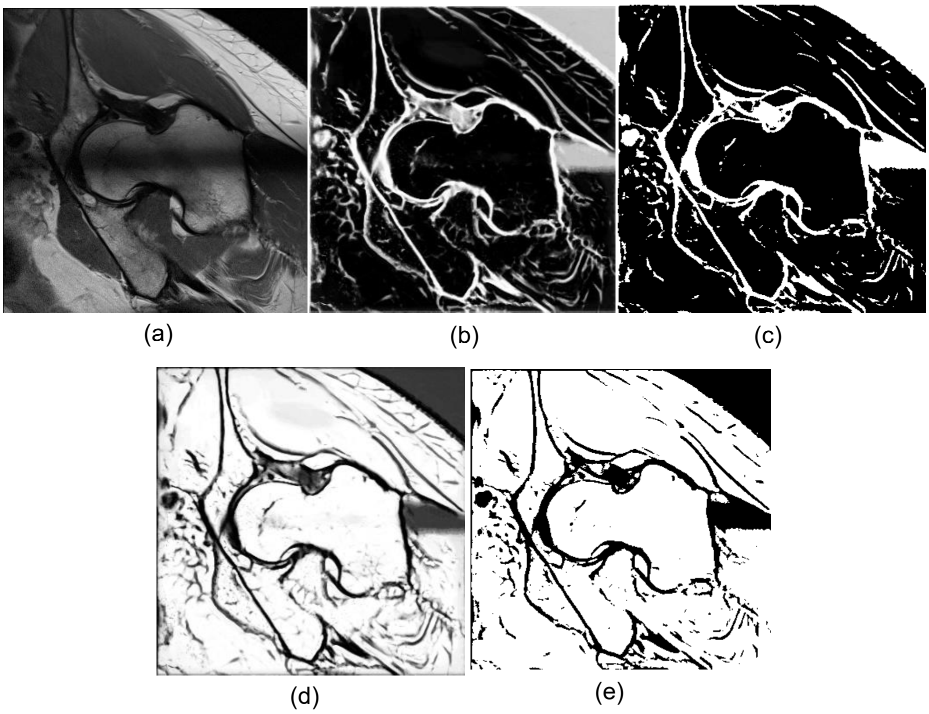

Figure 30 - (a) Original radial slice that was treated by the trained model. Output images after the application of the model of Pixel Classifier: (b) result of 1st class, (c) result of 1st class binarize (d) result of 2nd class (e) result of 2nd class binarize.

Considering Figure 30, looking at images b) and d), one can expect them to be more easily segmented using MATLAB® tools, namely *imerode*, *imreconstruct* and *imdilate*.

However, these methods only worked when they segmented the trabecular bone, as seen in Figure 31 – a), but not always due to errors during the previous step of pixel classification, where the crosstalk artifact was not totally removed (Figure 31 – b)) or due to the low contrast between femur and ligaments, which translates into lack of femur limits (Figure 31 – c)).

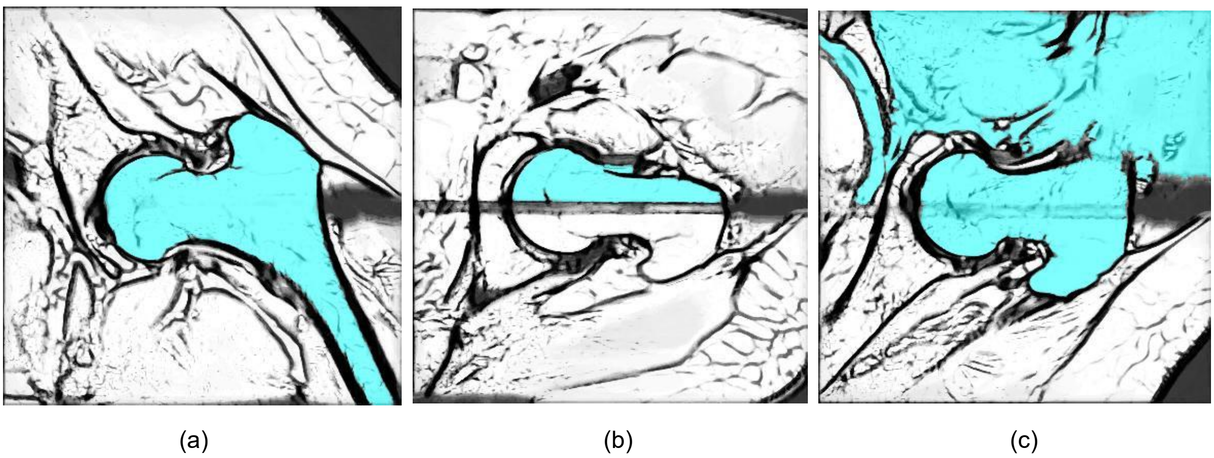

Figure 31 - (a) Successful segmentation of trabecular bone. (b) Unsuccessful segmentation due to crosstalk artifact. (c) Unsuccessful segmentation due to lack of femur limits.

Regarding to cortical bone, these simple segmentation tools did not work since the femur is inserted into the articular capsule, that in MRI it is very difficult to distinguish between different structures, such as cortical bone, tendons and ligaments, and after the step of classifying pixels all of these tissues were fused together, as Figure 32 shows.

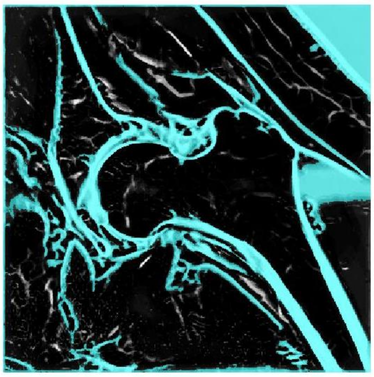

Figure 32 - Unsuccessful segmentation of cortical bone.

Based on B. R. Gomberg *et al.* [18], a distinct approach was attempted, illustrated in Figure 33, where starting from the border of trabecular bone in a perpendicular outward direction, using the normal vectors, the algorithm would collect some points of the cortical bone boundaries when reached a threshold difference corresponding to the transition between trabecular and cortical bone.

However, as can be seen in Figure 33 – b), there are several erroneous points collected as belonging to the cortical bone.

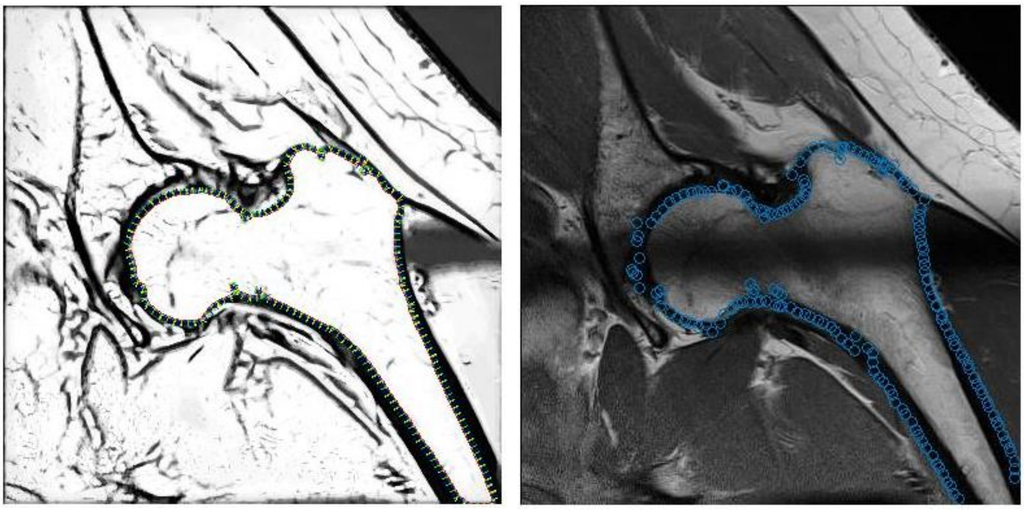

(a) (b)

Figure 33 - (a) Normal vectors around border of trabecular bone. (b) Points from cortical bone collected.

On the other hand, the femur segmentation from the radial sequence is intended to formulate its volume in 3D space through an interpolation. So, one other approach was to divide in two parts each 2D radial scan after removal of the crosstalk artifact zone and segment it separately, as shown in Figure 34. This could be a good way to address the crosstalk artifact obstacle, because only a small fraction of the femur would disappear, but it would appear during the volume interpolation. Nonetheless, these half-images had the same problem of low contrast between the structures around the femur and the small differences between cortical and trabecular bone which could not be overcome with the MATLAB® segmentation tools, resulting in non-precise edges of the femur and a non-accurate segmentation that is required.

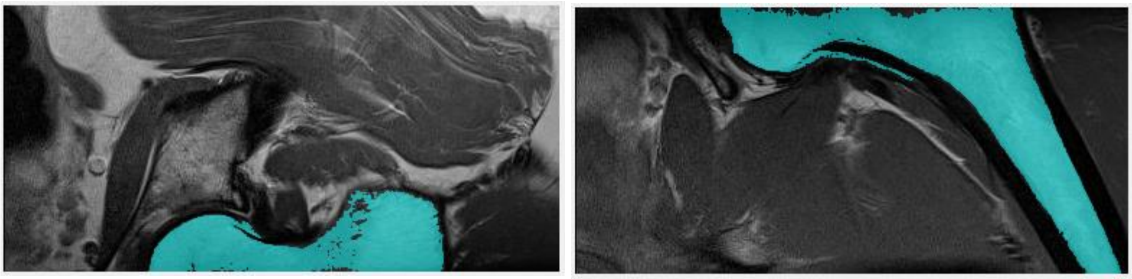

Figure 34 - Part of radial 2D scan and its segmentation.

Despite many attempts, it was not possible to obtain an automated segmentation of the femur within the radial sequence, due to many problems inherent to these MRI (crosstalk artifact and low contrast between structures present in the articular capsule).

Therefore, the manual segmentations of the 48 radial 2D scans were made, from which it was possible to develop its volume, as shown in Figure 35.

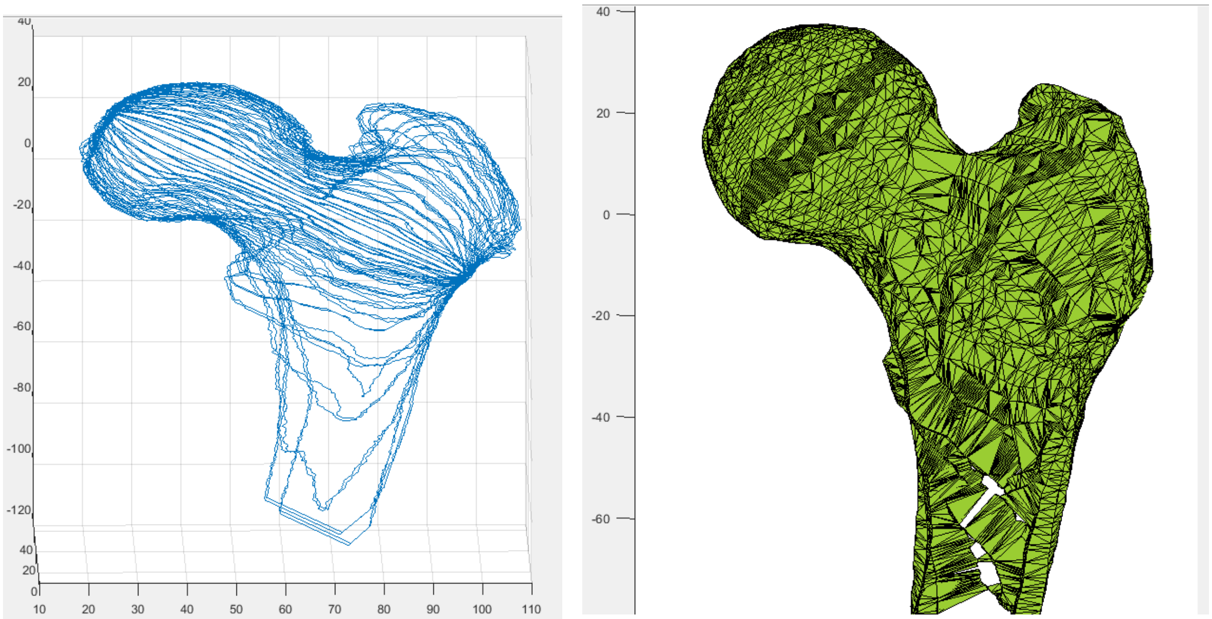

Figure 35 - Volume obtained after manual segmentation of the radial sequence.

3.4. Preoperative Planning Tool

This section presents the software application developed, including the steps that the user must follow to achieve higher performance.

3.4.1. Outline Region to Operate

To perform the preoperative planning of hip preserving surgery, an interactive application was developed in MATLAB® whose interface is illustrated in Figure 36. This GUI is divided into three sections: (1) file region where the user can load the DICOM files of the 2D radial sequence of a specific directory located on his computer; (2) presentation of each editable radial slice with interactive tools to delineate the region to operate; (3) 3D space in which the radial sequence is represented and also the interpolated surface of the region to be operated.

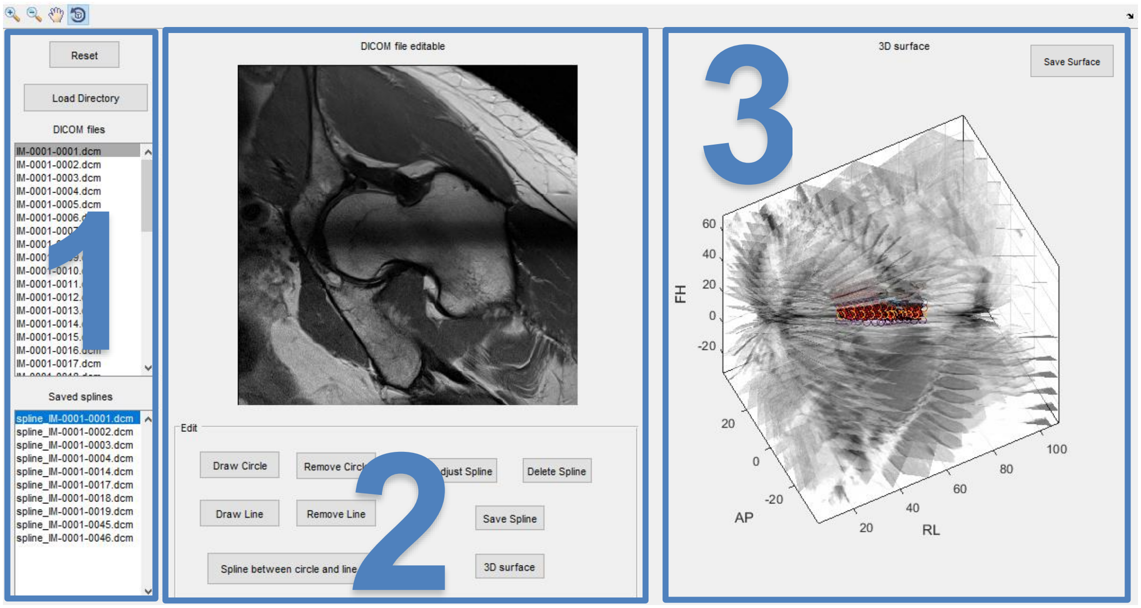

Figure 36 - GUI of an interactive application to outline the section to operate: (1) file region; (2) editable region; (3) viewing region of the 3D surface of the section to operate.

First, the user must choose the folder where the DICOM files are located on the computer by clicking the 'Load Directory' button. After that, the list with the original 2D radial sequence will appear, and if there is already any saved work, they will appear in a second listbox below, as exemplified in Figure 37.

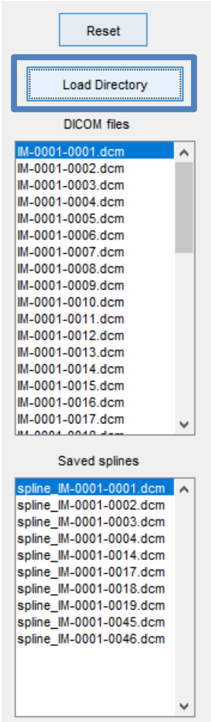

Figure 37 - File region

There is the possibility of starting a new trial with a completely different radial sequence to prepare the surgery of different patients by clicking the 'Reset' button, which allows the application to erase the listed files and any open image.

When the user clicks on a specific DICOM filename, its image will be visible in the editable region. Afterwards, he has the possibility to perform the delineation of the operative region. For that, he has two different tools at his disposal: a circle, because the main goal is to correct the non-sphericity of the femoral head, and a line to establish how the circle would be connected to the other part of the femoral head.

Figure 38 illustrates how the circle should be made. After clicking 'Draw circle' button, over the editable image, the cursor will change its appearance to a cross and the user will be responsible for clicking at least three different points of the image and then press the 'enter' key on the keyboard. The location of each point is very important since the circle will be drawn so that these points belong to the circumference. Thus, the user must choose peculiar points from the femur that characterize the desired sphericity of the bone that will undergo an operation.

Whenever the user is not satisfied with the drawn circle, he can delete it by clicking the 'Remove Circle' button.

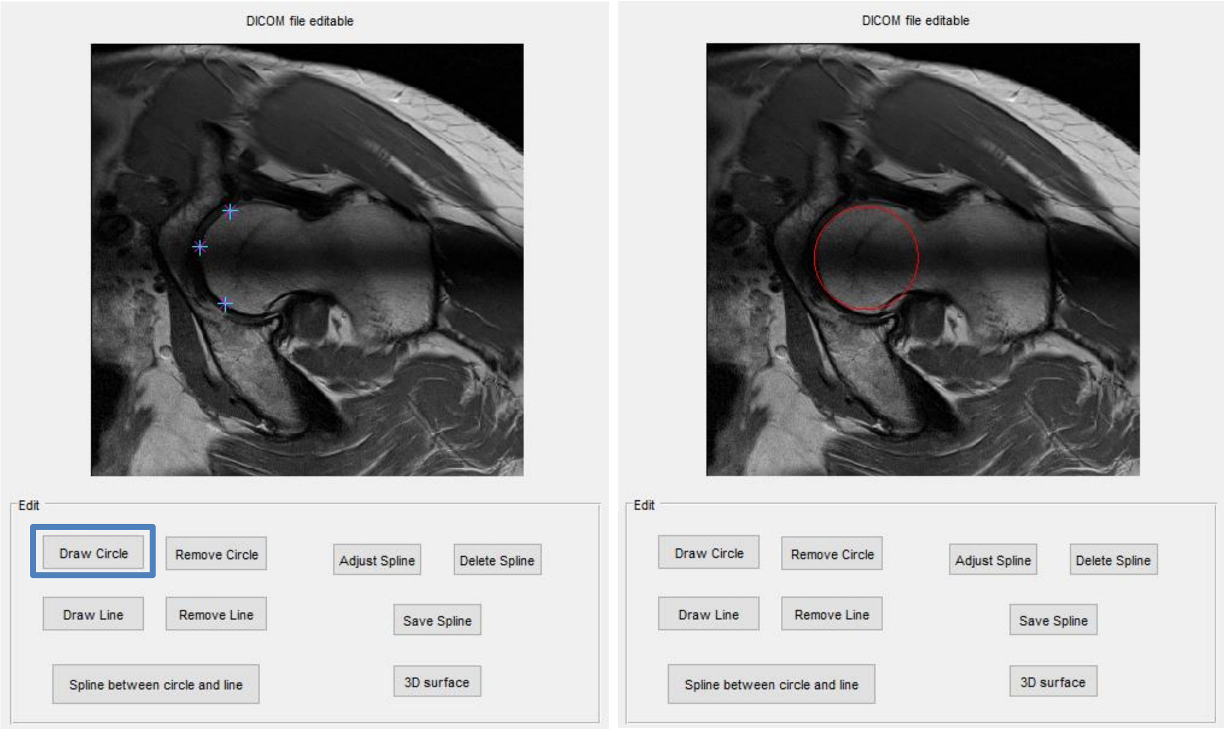

Figure 38 - Using the circle tool.

When the 'Draw Line' button is clicked, a small line will appear in the center of the editable image. The user should drag it to where he thinks the circle will line up with the remains of the femoral head, as shown in Figure 39 – a).

Then the user will click on the 'Spline between circle and line' button to create a blue line representing the section of bone to be operated, as displayed in Figure 39 – b). It is advisable to remove both circle and the line using the 'Remove Circle' and 'Remove Line' buttons as in Figure 39 – c).

The spline line can be easily adjusted by dragging several points that pop up when the user clicks the 'Adjust spline' button. Whenever any point within the line is moved, a red line follows the adjustments made so that the user can interactively change the contour of the region to operate, as shown in Figure 40.

When the user is satisfied with the current outline is expected to click the "Save Spline" button that will make it appear in the list of saved splines. At any time, the spline line can be removed by clicking on the 'Delete Spline' button.

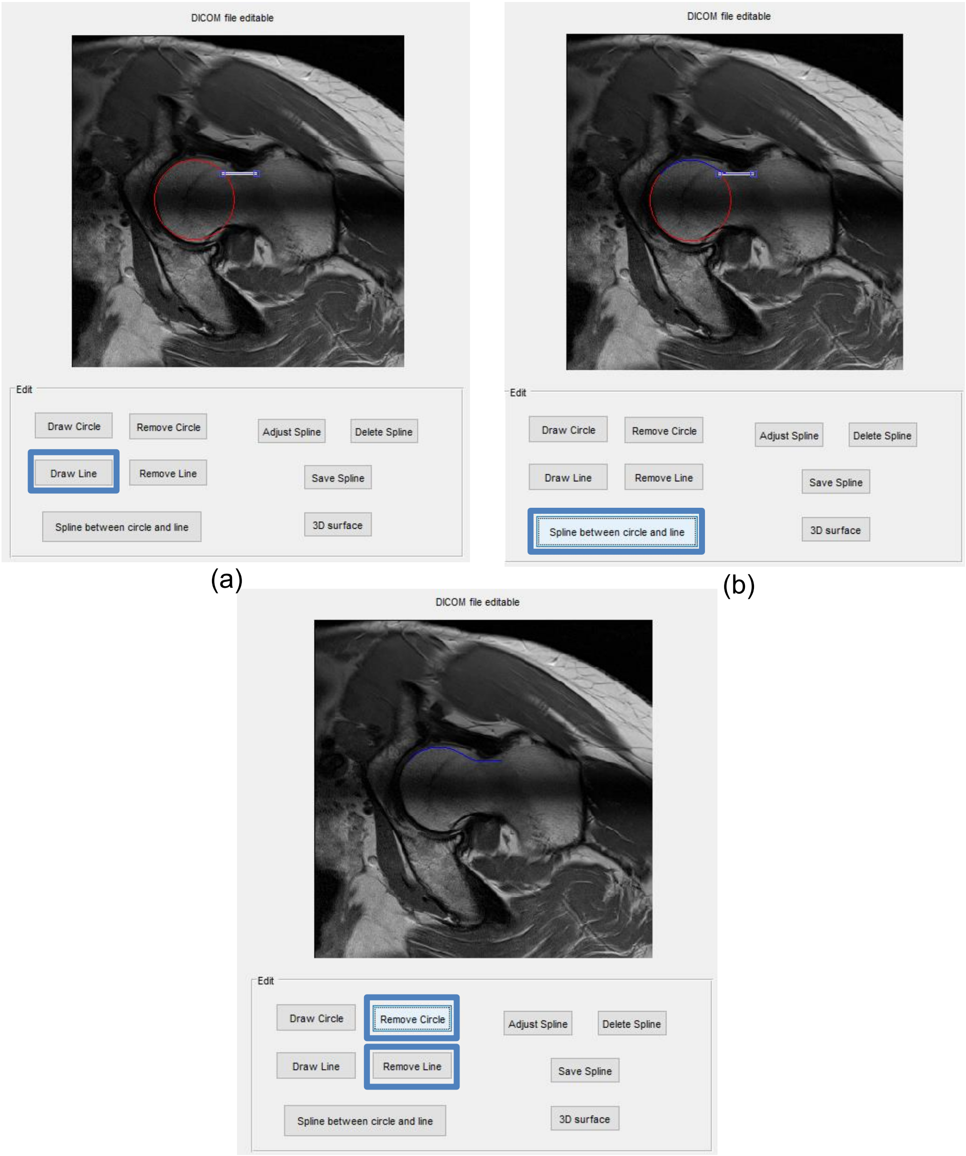

Figure 39 - Performing the spline.

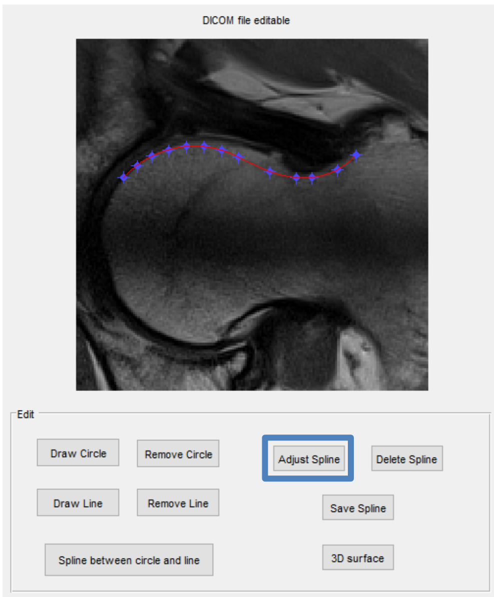

Figure 40 - Adjust spline.

In any moment, the user can see a spline already saved by clicking one of the filenames located in the list of saved splines, as illustrated in Figure 41. Here the spline line is light blue in color.

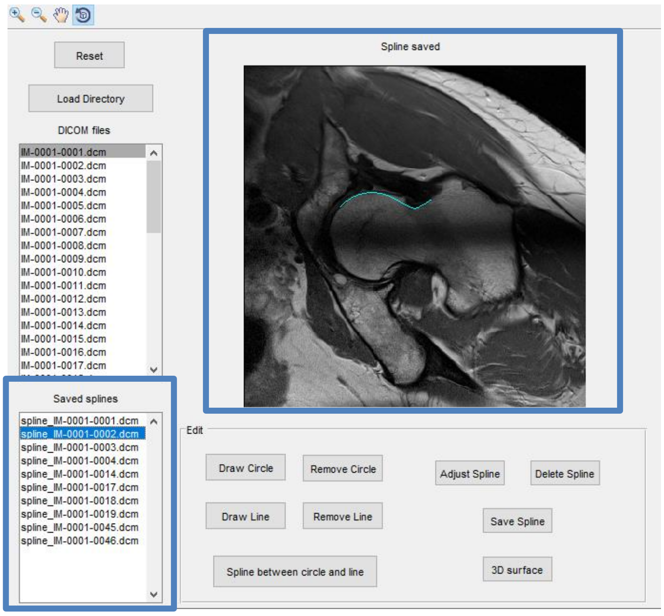

Figure 41 - Visualization of saved spline.

When the user has delineated several splines in different radial scans, he can press the '3D Surface' button, which will produce a 3D plot of the interpolated surface based on the points of diverse spline lines in red. Also, in the same 3D space it will be displayed all the slices of the 2D radial sequence, as shown in Figure 42.

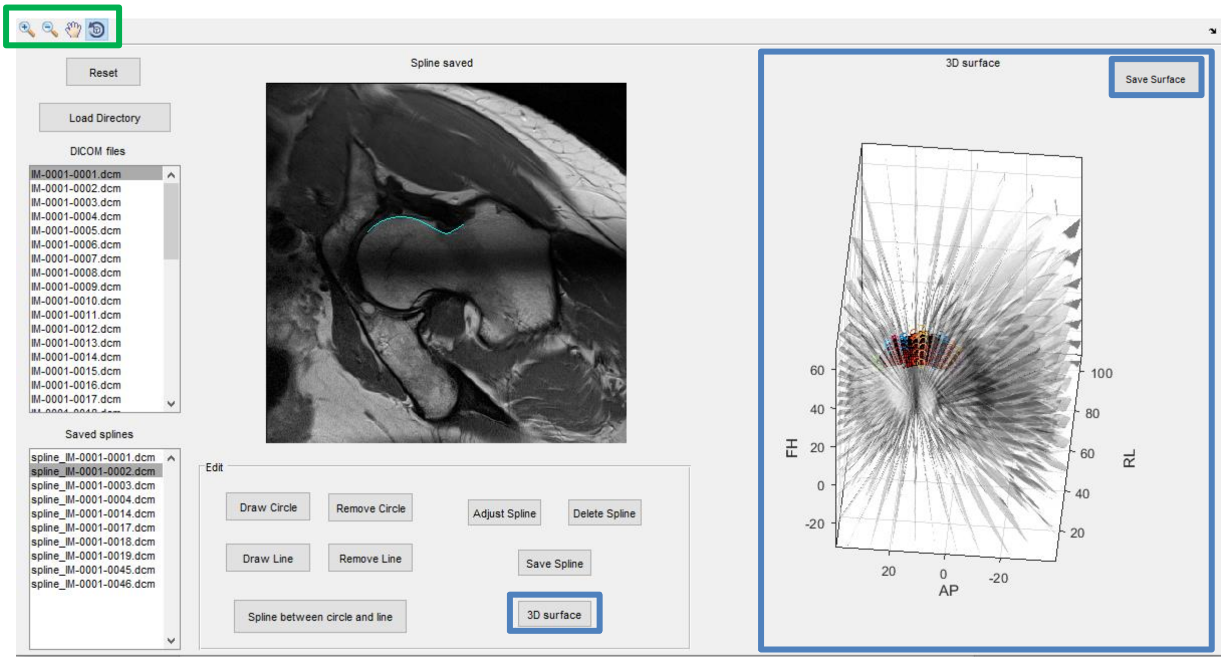

Figure 42 - 3D visualization of the radial sequence and the interpolated surface of the region to operate in red.

When the user is satisfied with the formulated surface, he can press the ‘Save Surface’ button, which will allow the user to save it to the computer in a *.mat* output file with all the characteristics related to the interpolated surface.

In addition, several familiar icons of MATLAB® figures have been added in the application in the upper left corner to allow the user to zoom in/out and drag any image with the mouse. Also, in the 3D graph, he can rotate the surface interactively. These icons are highlighted in the green box in Figure 42.

3.4.2. Principal Component Analysis (PCA)

To ensure that the interpolated surface generated by this application works correctly for each radial MRI sequence, it was necessary to resort to the Principal Component Analysis (PCA) method.

PCA is normally used to reduce the dimensionality of large data sets, maintaining most of the variation present in the original data set [34].

Principal components are new uncorrelated variables constructed as linear combinations of the initial variables and their order is made so that the first ones have the most information in terms of variation of the original variables. Geometrically, principal components correspond to the lines that capture most of the data information, because they represent the directions of the data that explain a maximum amount of variance [35].

By thinking the principal components as new axes that provide the best angle for viewing and evaluating data, the surface developed in the application presented in the previous section was implemented in this new reference frame.

MATLAB®’s *pca* function returns the principal component scores, which are the representations of the input data in the principal component space, being, in the developed application, the new coordinate values of the points collected from the splines drawn by the user. Thus, using the function *fit* of MATLAB® it was possible to create the surface through cubic piecewise interpolation ('cubicinterp' as ‘fitType’) for each case in its best principal component space. In this way, the femur of several patients, which translates into different radial MRI sequence in distinct patient’s coordinate system and, consequently, in particular pre-planned splines, it is possible to construct 3D surfaces of the regions to operate regardless and independently of their spatial location.

Hereafter, it was required to transform the surface of the principal component space into the original patient’s coordinate system so that it visually appears in the right place where the user pre-planned the section to operate the femur. For that, the transformation matrix was built through the rotation matrix and translation vector as presented in Equation (2), which described the transformation between the input data into the output scores of the *pca* function.

$$M = \begin{bmatrix} R_{11} & R_{12} & R_{13} & t_1 \\ R_{21} & R_{22} & R_{23} & t_2 \\ R_{31} & R_{32} & R_{33} & t_3 \\ 0 & 0 & 0 & 1 \end{bmatrix} \tag{2}$$

3.5. Registration

Once you have the 3D surface that outlines the section to operate based on the radial MRI sequence, it is required to merge the coordinate systems of that surface and the patient in the OR.

Being hip arthroscopy performed laparoscopically, one has to imagine that the surgeon would have to collect points along the surface of the unhealthy femur with a pointer, before correcting the cam type FAI.

This procedure was recreated in the lab with a real dimensions femur made of plastic stabilized on top of a table, using the NDI Polaris Spectra System, as shown in Figure 43.

(a)

(b)

Figure 43 - Setup for registration process. NDI Polaris Spectra System (a) facing towards the realistic plastic femur and pointer (b).

3.5.1. NDI Polaris Spectra System

NDI Polaris Spectra System (Northern Digital Incorporated, Waterloo, Ontario, Canada) is used in a variety of surgical applications by medical device manufacturers worldwide. It is based on optical measurement technology to determine the location and orientation of an object or tool on a particular coordinate system, "that delivers exceptional accuracy and reliability" [36].

In this work, it was implemented the optical tracking of passive markers, which are spherical markers which reflect infrared light, emitted by illuminators on the position sensor – Polaris spectra. These four reflecting spheres are allocated on the pointer, as presented in Figure 44. The location of its tip can be calculated by the position sensor through the position and orientation receive from the markers.

Figure 44 - Pointer with four reflecting spheres.

3.5.2. Pointer pivoting

Before starting to collect points on the surface of the plastic femur, it was necessary to compute the offset of the pointer tip through the collected positions of the spherical markers allocated in the tool. This procedure called pointer pivoting, is performed with the help of the NDI Polaris Track software.

After choosing the acquisition time in this software, the pointer tool should be rotated in a cone shape around the tip at an angle between 30 and 60 degrees to the vertical axis as shown in Figure 45. It is important to notice that the tool tip must be fixed, that is pinned to a stationary point, and the passive markers must always be unobstructed facing the Polaris system. In addition, the selected acquisition time must be long enough for Polaris to collect a high number of position acquisitions for the program to converge with minimal error. On the other hand, a longer period of time may be subject to greater user error.

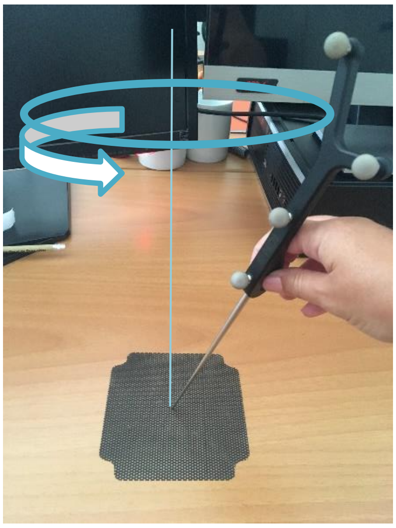

Figure 45 - Pointer pivoting.

3.5.3. Acquisition

Computed the offset of the pointer tip, data acquisition was performed. It was important to collect points from the plastic femur surface in the same region as the pre-planned surface created on the section 3.4.1. For this purpose, the boundaries of the section where the pointer tool should touch have been marked with tape carefully so as not to wrinkle the plastic surface so that the surface coverage would not be interrupted or the tip would not be lifted incorrectly.

In the NDI Polaris Track software, it was chosen for data acquisition 1 minute of time acquisition with 60 frames per second (maximum value permitted).

During this operation, the points on the plastic surface were attentively acquired in slow movements to ensure that the spherical markers are within the measurement volume that can be traced in the Polaris position sensor coordinate system and, also, correctly facing the sensor without obstacles so that their position can be tracked.

Completing this action results in a *.csv* output file that has 14 columns described on Table 3. From which, the only important information is the state regarding the quality of the recorded information and the spatial coordinates of the pointer tip (Tx, Ty, Tz). Only values corresponding to acquisition status "OK" have been accepted.

Table 3 - Columns and their description of the .csv output file

Column of the .csv file	Description
Tools	Number of tools tracked. (in this case 1 which is the pointer tool)
Port 1: NDI 8700340 s/n:34802401	Name of the tool.
Frame	Current frame (the software begins to acquire positions when it is turned on, but the user chooses whenever it starts to register them)
Face	Number of faces tracked. (in this case 1 since it is used a single-faced probe tool)
State	Acquisition state, which can be 'OK', 'Missing' or 'Too Few Markers' depending on field of view of the position sensor.
Quaternions (4 columns: Q0, Qx, Qy, Qz)	Representation of the orientations and rotations of the tool in three dimensions space.
Coordinates (3 columns: Tx, Ty, Tz)	Coordinates of the tip pointer.
Error	Error associated with acquired point positions.
Markers	Number of markers used on the tool.

3.5.4. Iterative Closest Point (ICP) Algorithm

After collecting points from the plastic femur surface, the registration between this point cloud and the pre-planned surface in section 3.4.1 was performed by applying the Iterative Closest Point (ICP) algorithm through the MATLAB® *pcregistericp* function.

The ICP algorithm, introduced by P. J. Besl and N. D. McKay [37], is described as the best alignment between a 'data' shape P with a 'model' shape X. Both represented in point sets, N_P and N_X denote the number of points in the data shape and model shape, respectively. This algorithm is initialized by defining the registration vectors relative to the initial data set P_0 to ensure that the final registration represents the complete transformation. The following steps are applied until convergence within a tolerance τ is reached.

1. Closest points are computed, meaning that is found the correspondence between each point of P to its nearest point of X.
2. The registration is computed so that translation *t* and rotation *R* minimize the sum of the squared error, where x_i and p_i are corresponding points:

$$E(R,t) = \frac{1}{N_P}\sum_{i=1}^{N_P} \|x_i - Rp_i - t\|^2 \qquad (3)$$

3. Registration is applied, i.e. transform the data set P with the transformation computed in the previous step:

$$P_{k+1} = RP_k - t \qquad (4)$$

4. The iteration terminates when the mean square error is lower than a preset threshold τ which specifies the precision desired for the registration:

$$d_k - d_{k+1} < \tau \qquad (5)$$

The mean square error designated as d_k is defined as:

$$d_k = \frac{1}{N_P}\sum_{i=1}^{N_P} \left\|x_{i,k} - p_{i,k+1}\right\|^2 \qquad (6)$$

The ICP algorithm relates two sets of points which may not have the same number of points, as is the case with this project: the point cloud collected with the Polaris pointer and the point cloud acquired from the user pre-planned surface. Also, ICP algorithm always converges monotonically to a local minimum corresponding to the best transformation that aligns one point cloud to another.

4. Results and Discussion

In Section 3.4.1, it is shown how the user can obtain a 3D interpolated surface corresponding to the region to be operated. Figure 46 shows that surface within the volume obtained after manual segmentation of the MRI radial sequence performed in section 3.3. It is noteworthy the correction of the femoral head contour in which its sphericity is recovered.

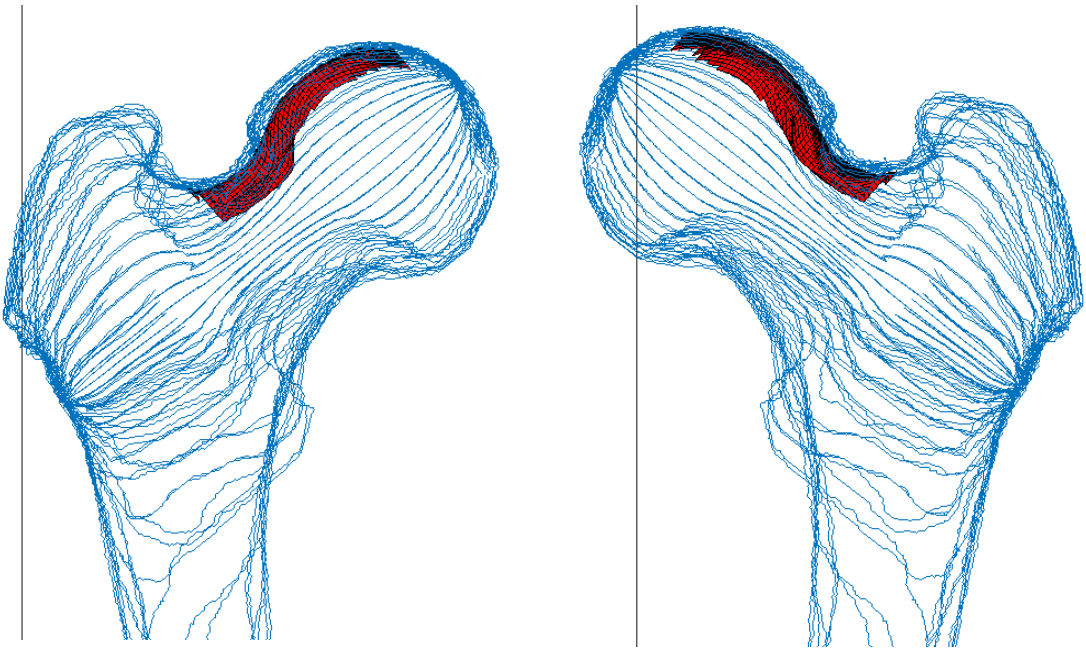

Figure 46 - 3D volume of manual segmentation of the femoral head with the interpolated surface.

4.1. Region Validation

The 3D surface that is interpolated based on the splines drawn by the user is created through a piecewise cubic interpolation function from MATLAB®. This method fits a different cubic polynomial between sets of three points for surfaces.

To ensure that this technique is functional for the purpose of delineating the region to operate, this application was used to segment some portion of the femoral head to verify if it would correspond to the real surface of the femur that is available in the T1 axial MRI set, illustrated in Figure 47.

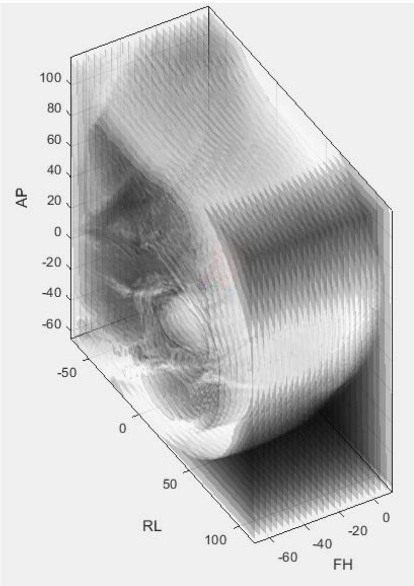

Figure 47 - T1 Axial MRI.

In Figure 48 it is possible to observe on the left one of the splines performed in one of the radial scans that translate the segmentation of the femoral head and to its right the interpolated 3D surface. Consecutive radial scans were used to ensure that the interpolated surface between them resemble the contour of the true femoral head.

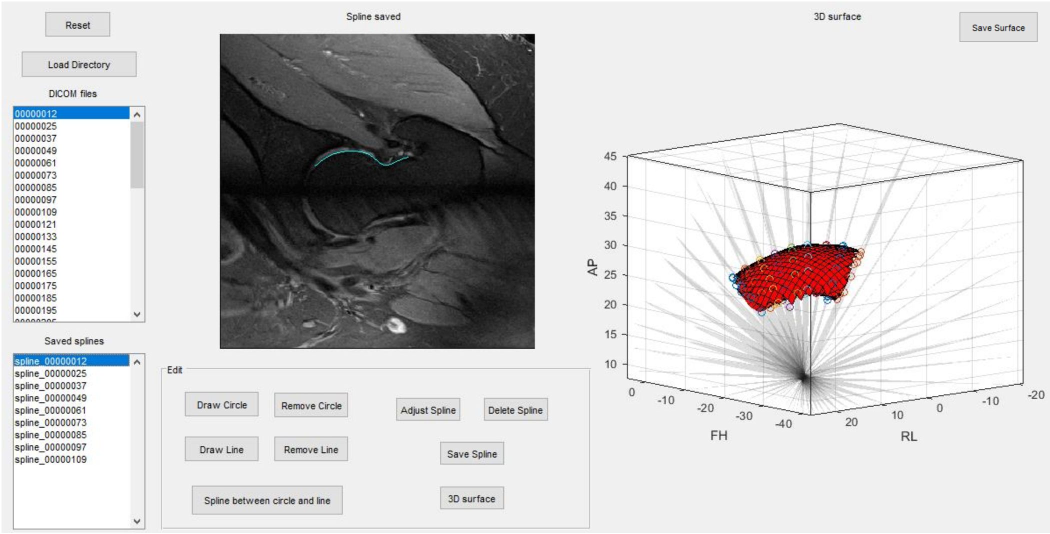

Figure 48 - Delineate the segmentation.

Figure 49 displays in red the interpolated surface within axial MRI set. The different viewing angles allow to confirm that the cubic spline interpolation method is acceptable to define surfaces from points of multiple spline lines acquired from radial slices.

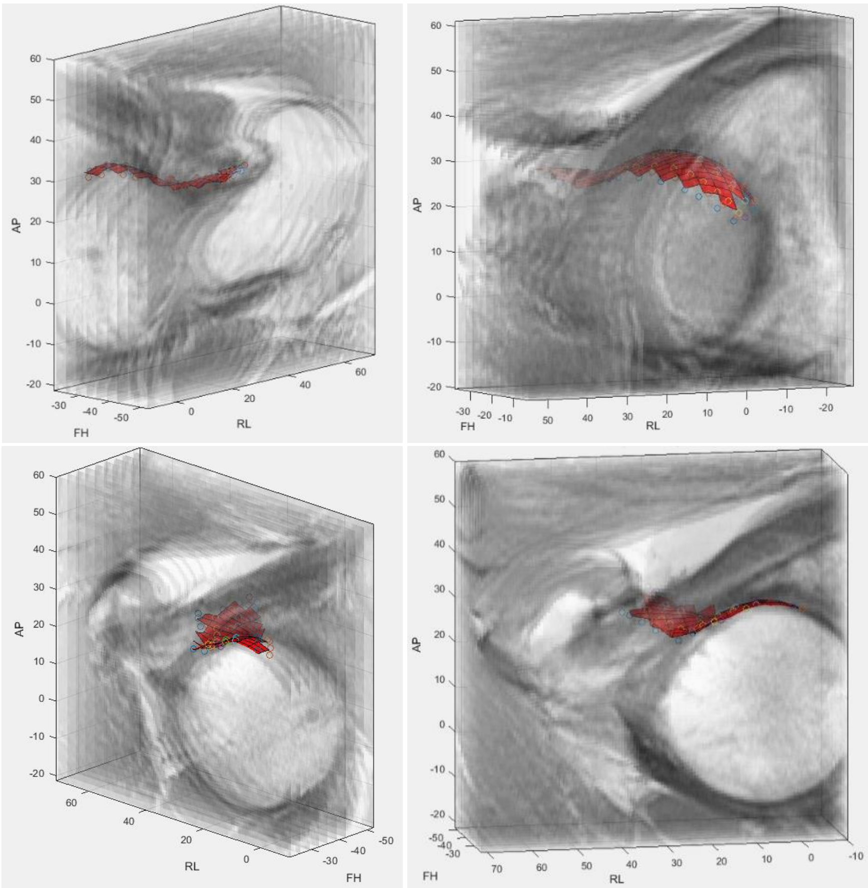

Figure 49 - Interpolated surface within the T1 axial set from different viewing angles.

To further evaluate whether the developed surface recreates the true surface of the femur, another interactive application has been developed where it is possible to further explore the 3D coordinate system of the two MRI sets (radial and axial).

As shown in Figure 50, the layout is divided into four sections: (1) file region where the user can load the DICOM files of the 2D radial and axial sequence from a specific directory located on his computer and also load the surface output MATLAB® file created on the section 3.4.1; (2) presentation of each 2D slice already loaded (radial, axial or radial with the drawn spline slices); (3) 3D space in which the radial or axial MRI sequence is represented, the interpolated surface of the region to be operated in red and in blue the plane schema represented in the following section; (4) surface presentation in the same 3D space as specific transverse femur planes or axial planes.

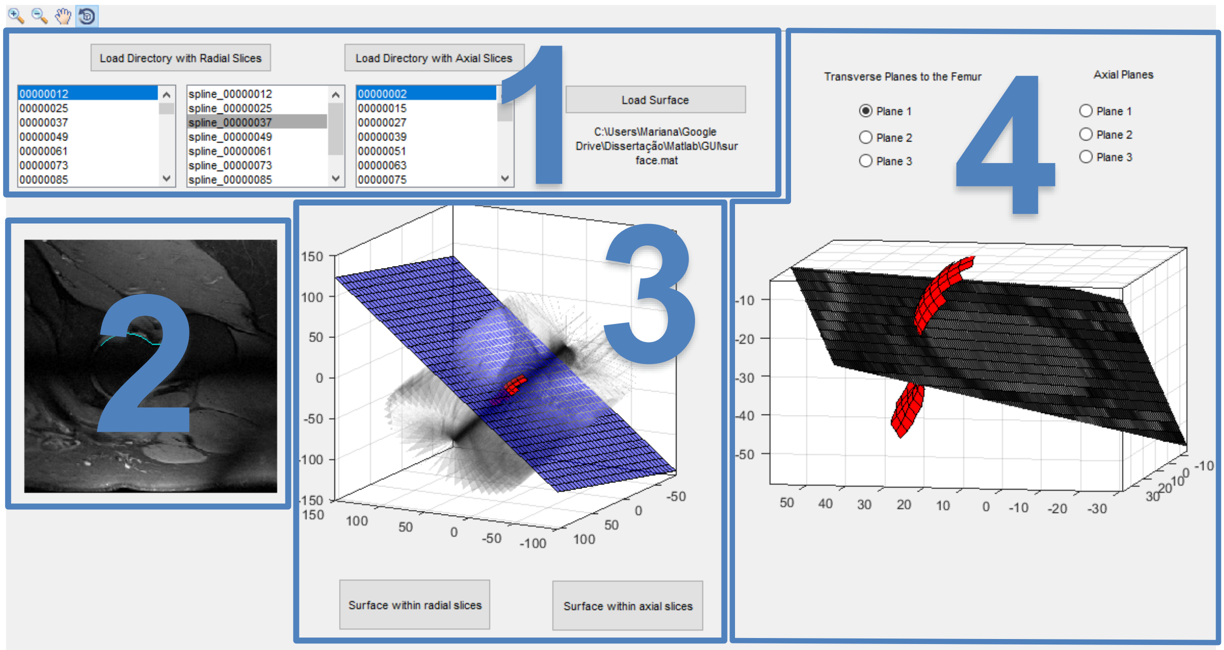

Figure 50 - Interactive application to evaluate the developed surface within the MRI sequences: (1) file region; (2) 2D plane; (3) viewing region of the 3D surface of the section to operate within radial or axial MRI sequence (4) viewing region of the 3D surface of the section to operate within specific transverse or axial planes.

There are three possible transverse planes to the femoral head/neck that were created by the intersecting the 26 axial MRI slices with these previously chosen planes. That is, a new transverse slice was created through the intensity values of the pixels collected from the axial sequence at each intersection, as illustrated in Figure 51. These three planes have a vertical resolution of 3mm, as it corresponds to the distance between consecutive axial slices of the T1 MRI set. In the horizontal direction, it is possible to have a better resolution of approximately 0.7mm, equal to each axial slice. Thus, resulting in a transverse slice that looks like pixelated rectangles with worse vertical resolution. Nevertheless, the intersection between the red developed surface with each transverse plane confirms that the surface represents the true femoral surface.

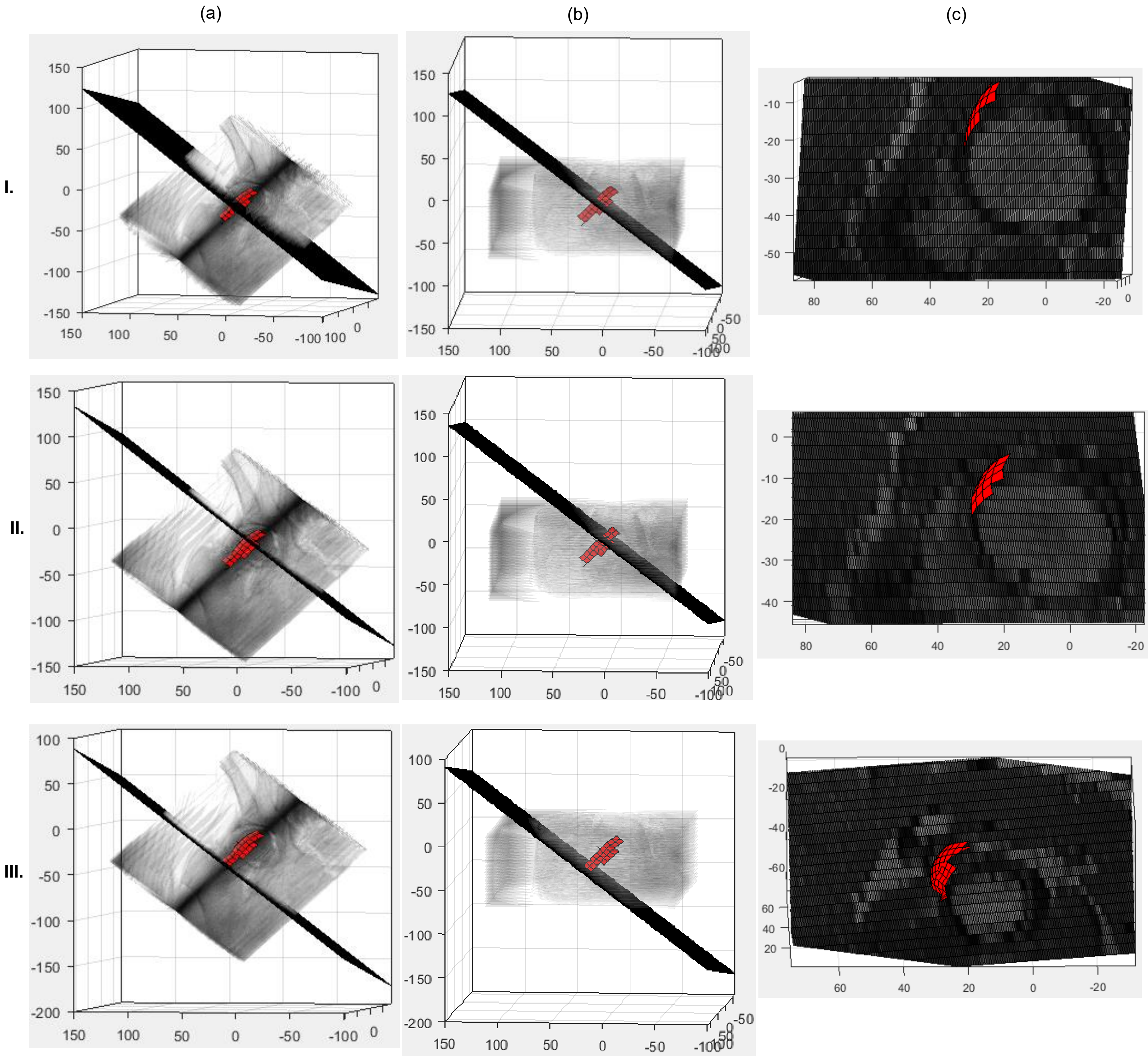

Figure 51 – First (I.), second (II.) and third (III.) transverse planes generated. (a) radial MRI sequence, surface and schema of the transverse plane in this 3D space. (b) axial MRI sequence, surface and schema of the respective transverse plane in this 3D space. (c) transverse plane created and surface overlap.

In addition, three axial planes from the MRI sequence were selected for further analysis of the developed surface to confirm that it corresponds to the actual femoral surface. Considering Figure 52, it is noticeable how the red surface follows the contour of the femur on each axial slice, confirming that the technique used to create and interpolate this surface can be accepted to pre-plan the region to operate for cam type FAI correction, qualitatively.

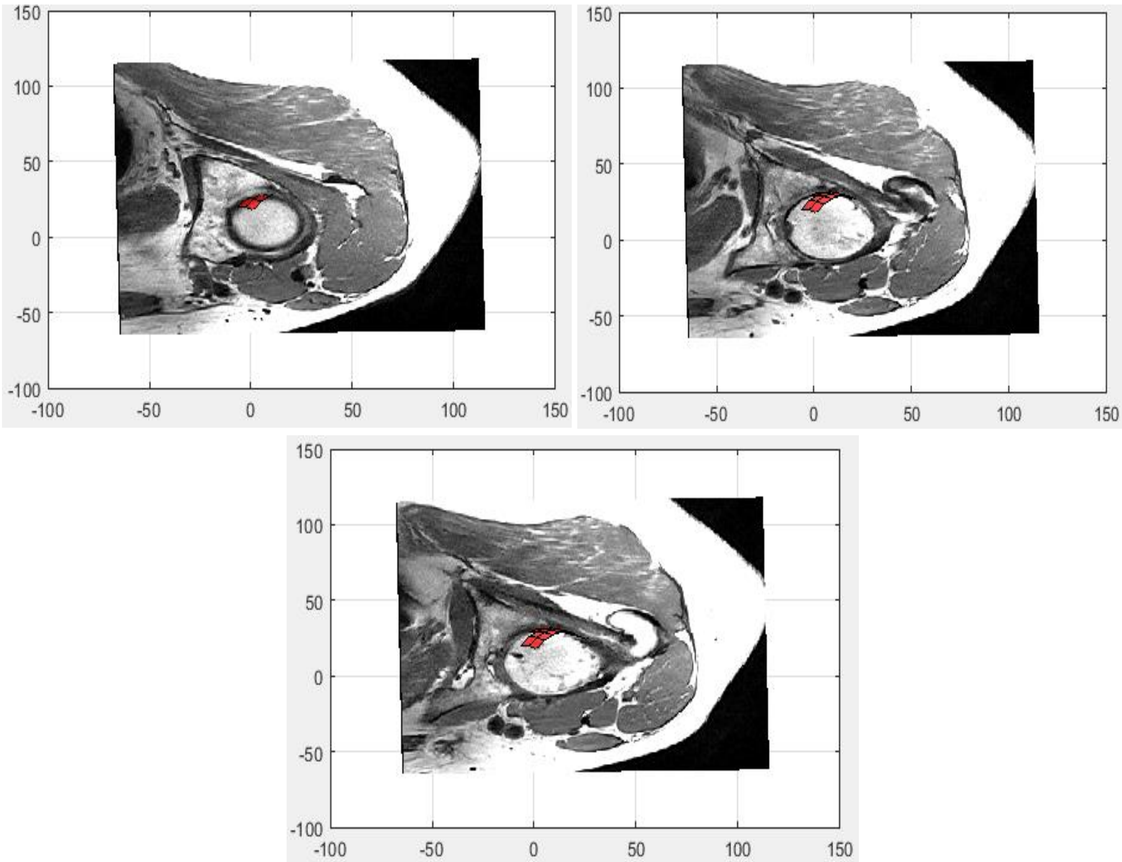

Figure 52 - Three selected axial planes represented with the surface corresponding to the real femoral surface.

4.2. Registration

This section presents the results after applying the ICP algorithm to perform the registration between the points collected from the plastic surface using the Polaris position sensor and the tool pointer and the point cloud acquired from the surface developed in section 3.4.1.

Figure 54 illustrates the two point clouds in the same 3D space before registration, where the points from the developed surface are represented in green, considered as the fixed point set, and the purple points portray all coordinates points of the pointer tip position along the plastic surface femur, treated as the moving point cloud. Figure 53 illustrates these two point clouds after registration, where it was not use any initial transform and the ‘minimization metric’ used was the default ‘pointtopoint’ option of the MATLAB® *pcregistericp* function .

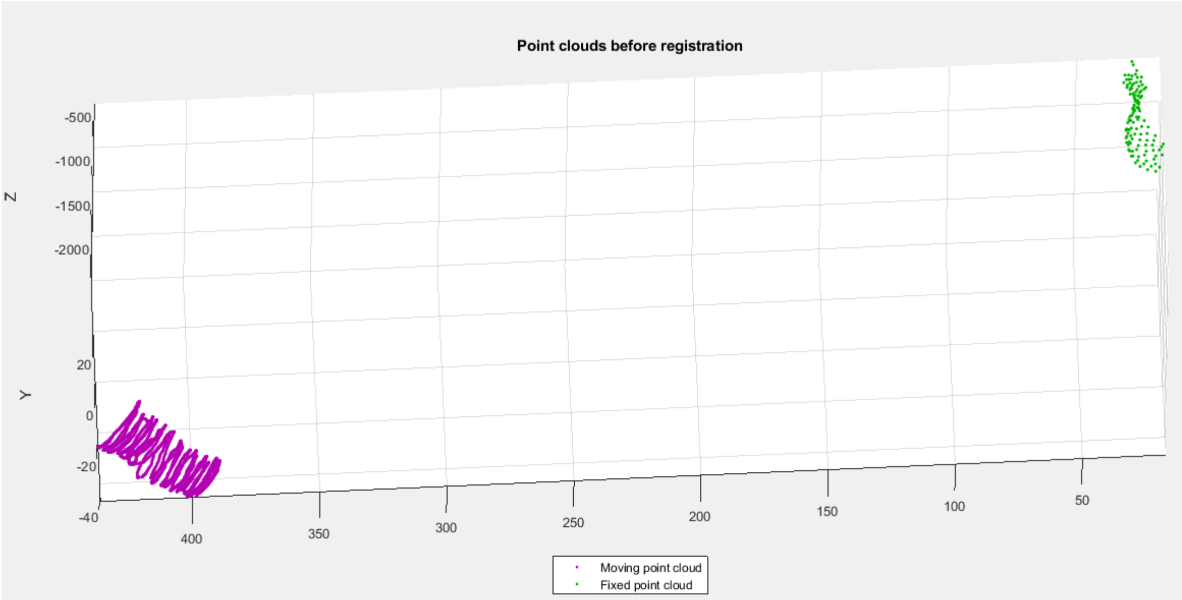

Figure 54 - Both point clouds before registration.

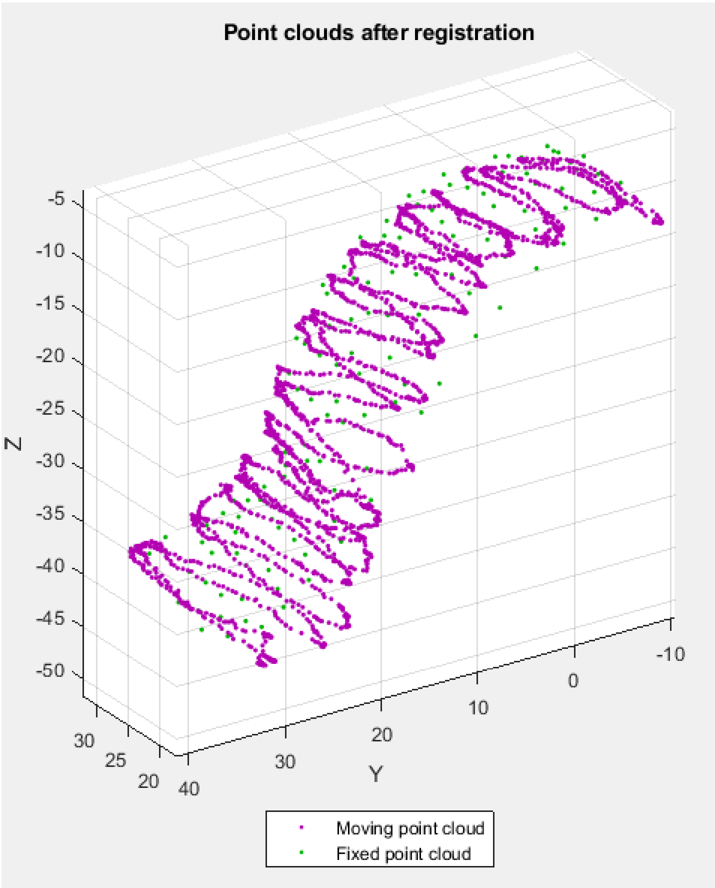

Figure 53 - Both point clouds after registration using ICP algorithm.

In addition, it was used the default stop criteria of the MATLAB® *pcregistericp* function. The ICP algorithm stops when the average difference between estimated rigid transformations in the three most recent consecutive iterations is less than the stipulated tolerance value. The tolerance between consecutive ICP iterations used was:

$$[T_{diff}\ , R_{diff}] = [0.01, 0.05] \qquad (7)$$

This 2-element vector represent the absolute difference in translation and rotation estimated in successive iterations. While T_{diff} determines the Euclidean distance between two translation vectors, R_{diff} measures the angular difference in degrees.

The resulting transformation matrix computed through the ICP algorithm was:

$$M = \begin{bmatrix} 0.8 & 0 & 0.6 & 1330.1 \\ -0.6 & 0 & 0.8 & 1614.8 \\ 0 & -1 & 0 & 395.4 \\ 0 & 0 & 0 & 1 \end{bmatrix} \qquad (8)$$

and the Euclidean distance between the aligned point clouds, designated as root mean square error (RMSE) was:

$$RMSE = 2.2616\ mm \qquad (9)$$

The error may be related to the fact that the point clouds used do not represent the same object. While one was collected from the plastic surface representing a healthy bone using the pointer tool, as explained in section 0, the other was acquired from the surface developed in section 3.4.1. based on a radial MRI sequence from a cam type FAI patient diagnosis.

However, the ICP algorithm was able to perform the registration as it can work on data sets with different number of points and without any correspondence between them. Therefore, no additional steps in the process requiring the identification of points from different point clouds was necessary.

5. Conclusion

The main goal of the work established in this thesis was to develop a preoperative planning tool to be part of a robot-assisted conservative hip surgery procedure to correct the cam type FAI.

Although the application was initially designed as a compilation of the image processing tools available in MATLAB® and 3D slicer, the resulting software build solely on MATLAB® code proved to be capable of being the initial stage of the preoperatory procedure that the orthopedic surgeon would have to perform in this innovative surgery.

As the use of radial MRI sequence was the differentiating factor in the creation of this new preoperative planning tool when compared to the existing procedures presented in the subsection 'State of the art', as it is used as the main imaging study during the diagnosis of this medical condition and the 3D volume created from the 2D scans did not have the best resolution, it was necessary to work on each radial slice one at a time.

Unfortunately, the objective of femur segmentation from radial images could not be performed automatically and had to be done manually.

Nevertheless, the interactive application developed allowed the user to outline the contour of a healthy femoral head over each 2D radial view of the unhealthy femur, allowing the user to recreate the lost sphericity due to the cam type FAI in a user-friendly and easy-to-view manner, since the user can easily drag certain points belonging to the spline line that moves along the user's indications.

In addition, the software developed can successfully create the surface that can be used as a safety zone on which the robot arm will be constrained to work, as it can also recreate the real surface of the unhealthy femur after delineating a part of the femoral head present in the 2D MRI sequence, validating the use of the piecewise cubic interpolation function.

Finally, the last objective which was the registration between the surface formulated on the application and the surface of the femoral head was complete, by mimicking the operating room conditions in which it was required to collect the point cloud along the surface of a real dimensions femur made of plastic with the help of the optical measurement technology NDI Polaris Spectra System with its pointer tool and calculated using the Iterative Closest Point algorithm with an error on the order of $2mm$.

Certainly, these good results are optimistic from the perspective of laboratory practice, which means that for clinical practice, further studies are needed.

5.1. Future work

The work developed on this project is merely the beginning of the preoperative planning procedure for conservative robotic hip surgery and new developments are naturally needed to implement this innovative process in the operating room with a robotic arm. This includes the configuration required to integrate the interpolated surface created in the application here presented in the robot workspace, since it should be the safety zone and prevent the orthopedic surgeon from removing excessive bone from the femoral head when correcting the non-sphericity of a patient’s femur with cam type FAI.

Furthermore, the methods used throughout this work can be improved for better results, such as:

- configure a 3DSlicer MRI radial sequence DICOM reader;
- develop an automatic femur segmentation algorithm for the MRI radial sequence;
- improve 3D volume construction based on the MRI radial sequence;
- delineate the surface of the region to be operated by adjusting the best sphere in the 3D volume of the unhealthy femoral head;
- new techniques to perform the registration between the real unhealthy surface of the patient's femur in the operating room and the preoperative planned surface.

6. References

[1] F. Yu, L. Li, H. Teng, D. Shi, and Q. Jiang, “Robots in orthopedic surgery,” *Ann. Jt.*, vol. 3, no. 3, Mar. 2018.

[2] J. E. Lang *et al.*, “Robotic systems in orthopaedic surgery,” *J. Bone Jt. Surg.*, vol. 93-B, no. 10, pp. 1296–1299, Oct. 2011.

[3] M. Tannast *et al.*, “Computer-assisted Simulation of Femoro-acetabular Impingement Surgery,” in *Navigation and Minimally Invasive Surgery: Total Arthroplasty*, 2007, pp. 448–455.

[4] W.-Y. Lee, C. Kang, D.-S. Hwang, J.-H. Jeon, and L. Zheng, “Descriptive Epidemiology of Symptomatic Femoroacetabular Impingement in Young Athlete: Single Center Study,” *Hip Pelvis*, vol. 28, no. 1, pp. 29–34, 2016.

[5] K. Atesok, D. Galos, L. M. Jazrawi, and K. A. Egol, “Preoperative Planning in Orthoapedic Surgery,” *Bull. Hosp. Joint Dis.*, vol. 73, no. 4, pp. 257–268, 2015.

[6] D. P. Byrne, K. J. Mulhall, and J. F. Baker, “Anatomy & Biomechanics of the Hip,” *Open Sport. Med. J.*, vol. 4, pp. 51–57, 2010.

[7] O. Jones, “The Hip Joint,” *TeachMe Anatomy*, 2019. [Online]. Available: https://teachmeanatomy.info/lower-limb/joints/hip-joint/. [Accessed: 22-Jul-2019].

[8] F. W. Gwathmey and D. Lewis, “Femoroacetabular Impingement in the Adolescent Athlete,” *Oper. Tech. Sports Med.*, pp. 1–7, Apr. 2019.

[9] P. Emary, “Femoroacetabular impingement syndrome: a narrative review for the chiropractor,” *J. Can. Chiropr. Assoc.*, vol. 54, no. 3, pp. 164–176, 2010.

[10] C. E. Haldane, S. Ekhtiari, D. de Sa, N. Simunovic, and O. R. Ayeni, “Preoperative physical examination and imaging of femoroacetabular impingement prior to hip arthroscopy-a systematic review,” *J. Hip Preserv. Surg.*, vol. 4, no. 3, pp. 201–213, Jun. 2017.

[11] R. Nasser and B. Domb, “Hip arthroscopy for femoroacetabular impingement.,” *EFORT Open Rev.*, vol. 3, pp. 121–129, Apr. 2018.

[12] P. A. Rego, “Artroscopia da anca - Cirurgia Conservadora Anca,” 2016. [Online]. Available: https://www.cirurgiaconservadoraanca.com/pt/tecnicas-cirurgicas/artroscopia-da-anca. [Accessed: 23-Jul-2019].

[13] A. Webb, *Introduction to Biomedical Imaging*, IEEE Press Series on Biomedical Engineering, pp. 157-158, 2003.

[14] N. B. Smith and A. Webb, *Introduction to Medical Imaging,* Cambridge University Press, pp. 204-272, 2011.

[15] D. J. Bell and J. R. Ballinger, “MRI physics,” 2019. [Online]. Available: https://radiopaedia.org/articles/mri-physics?lang=us. [Accessed: 03-Sep-2019].

[16] L. Mullen and A. P. F. Gaillard, “MRI sequences (overview),” 2019. [Online]. Available: https://radiopaedia.org/articles/mri-sequences-overview?lang=us. [Accessed: 03-Sep-2019].

[17] N. Sugano, “Computer-assisted orthopedic surgery,” *J. Orthop. Sci.*, vol. 8, pp. 442–448, 2003.

[18] B. R. Gomberg, P. K. Saha, and F. W. Wehrli, “Method for cortical bone structural analysis from magnetic resonance images.,” *Acad. Radiol.*, vol. 12, no. 10, pp. 1320–1332, Oct. 2005.

[19] H. Chen *et al.*, “Automated segmentation of trabecular and cortical bone from proton density weighted MRI of the knee,” *Med. Biol. Eng. Comput.*, vol. 57, no. 5, pp. 1015–1027, May 2019.

[20] J. Schmid *et al.*, “Segmentation of the proximal femur in radial MR scans using a random forest classifier and deformable model registration,” *Int. J. Comput. Assist. Radiol. Surg.*, vol. 14, no. 3, pp. 545–561, Mar. 2019.

[21] G. Zheng and L. P. Nolte, “Computer-Assisted Orthopedic Surgery: Current State and Future Perspective,” *Front. Surg.*, vol. 2, no. 66, Dec. 2015.

[22] J. Liu *et al.*, “Review of Image Registration in Medical Robotics and Intelligent Systems: Fundamentals and Applications,” *Adv. Intell. Syst.*, 2019.

[23] N. Kobayashi *et al.*, “Computer-Assisted Hip Arthroscopic Surgery for Femoroacetabular Impingement,” *Arthrosc. Tech.*, vol. 7, no. 4, pp. e397–e403, Apr. 2018.

[24] C. N. Park *et al.*, “Robotic-assisted femoral osteochondroplasty is more precise than a freehand technique in a Sawbone model,” *J. Hip Preserv. Surg.*, vol. 2, no. 2, pp. 136–144, Jul. 2015.

[25] M. Masjedi *et al.*, “Use of robotic technology in cam femoroacetabular impingement corrective surgery,” *Int. J. Med. Robot. Comput. Assist. Surg.*, vol. 9, pp. 23–28, Mar. 2013.

[26] A. Kassarjian *et al.*, “Guidelines for MR Imaging of the Hip Region,” in *MRI of the Hip*, 2016, pp. 271–280.

[27] E. Venturi and A. Contri, “Radial MRI sequences of the hip: A study about how to perform radial sequences of the hip and about the diagnostic benefits.,” 2014.

[28] C. N. Petchprapa *et al.*, “Demystifying Radial Imaging of the Hip,” *RadioGraphics*, vol. 33, pp. E97–E112, 2013.

[29] D. Hitt and M. van Meel, “Acetabular radial hip imaging,” *F. Strength*, no. 38, pp. 42–45, 2009.

[30] J. Blackledge and A. Al-Rawi, “Stegacryption of DICOM Metadata,” *IET ISSC*, no. 26–27, Jun. 2014.

[31] R. N. J. Graham, R. W. Perriss, and A. F. Scarsbrook, “DICOM demystified: A review of digital file formats and their use in radiological practice,” *Clin. Radiol.*, vol. 60, pp. 1133–1140, 2005.

[32] P. Teodoro, “Robust Surface Reconstruction and US Bone Registration for Hip Resurfacing Surgery,” 2015.

[33] Innolitics, “DICOM Standard Browser,” 2018. [Online]. Available: https://dicom.innolitics.com/ciods. [Accessed: 06-Aug-2019].

[34] I. T. Jolliffe, *Principal Component Analysis*, Second Edi. Springer, 2002.

[35] “A step by step explanation of Principal Component Analysis.” [Online]. Available: https://towardsdatascience.com/a-step-by-step-explanation-of-principal-component-analysis-b836fb9c97e2. [Accessed: 16-Aug-2019].

[36] N. Medical, “Medical Polaris Spectra and Vicra.” [Online]. Available: https://www.ndigital.com/medical/products/polaris-family/. [Accessed: 13-Aug-2019].

[37] P. J. Besl and N. D. McKay, “A Method for Registration of 3-D Shapes,” *IEEE Trans. Pattern Anal. Mach. Intell.*, vol. 14, no. 2, pp. 239–256, Feb. 1992.